

First Results from the HI Jodrell All Sky Survey: Inclination-Dependent Selection Effects in a 21-cm Blind Survey

Robert H. Lang¹, Peter J. Boyce², Virginia A. Kilborn³, Robert F. Minchin¹,
Michael J. Disney¹, Christine A. Jordan³, Marco Grossi¹, Diego A. Garcia¹,
Ken C. Freeman⁴, Steven Phillipps² and Alan E. Wright⁵

¹*Department of Physics and Astronomy, Cardiff University, P.O. Box 913, Cardiff, CF24 3YB*

²*Astrophysics Group, Department of Physics, University of Bristol, Tyndall Avenue, Bristol, BS8 1TL*

³*Jodrell Bank Observatory, University of Manchester, Macclesfield, Cheshire, SK11 9DL*

⁴*Research School of Astronomy and Astrophysics, Mount Stromlo Observatory, Cotter Road, Weston, ACT 1611, Australia*

⁵*Australia Telescope National Facility, CSIRO, P.O. Box 76, Epping, NSW 1710, Australia*

Accepted ????. Received ????

ABSTRACT

Details are presented of the HI Jodrell All Sky Survey (HIJASS). HIJASS is a blind neutral hydrogen (HI) survey of the northern sky ($\delta > 22^\circ$), being conducted using the multibeam receiver on the Lovell Telescope (FWHM beamwidth 12 arcmin) at Jodrell Bank. HIJASS covers the velocity range -3500 km s^{-1} to 10000 km s^{-1} , with a velocity resolution of 18.1 km s^{-1} and spatial positional accuracy of ~ 2.5 arcmin. Thus far about 1115 deg^2 of sky have been surveyed. The average rms noise during the early part of the survey was around 16 mJy beam^{-1} . Following the first phase of the Lovell telescope upgrade (in 2001), the rms noise is now around 13 mJy beam^{-1} . We describe the methods of detecting galaxies within the HIJASS data and of measuring their HI parameters. The properties of the resulting HI-selected sample of galaxies are described. Of the 222 sources so far confirmed, 170 (77 per cent) are clearly associated with a previously catalogued galaxy. A further 23 sources (10 per cent) lie close (within 6 arcmin) to a previously catalogued galaxy for which no previous redshift exists. A further 29 sources (13 per cent) do not appear to be associated with any previously catalogued galaxy. The distributions of peak flux, integrated flux, HI mass and cz are discussed. We show, using the HIJASS data, that HI self-absorption is a significant, but often overlooked, effect in galaxies with large inclination angles to the line of sight. Properly accounting for it could increase the derived HI mass density of the local Universe by at least 25 per cent. The effect this will have on the shape of the HI Mass Function (HIMF) will depend on how self-absorption affects galaxies of different morphological types and HI masses. We also show that galaxies with small inclinations to the line of sight may also be excluded from HI-selected samples, since many such galaxies will have observed velocity-widths which are too narrow for them to be distinguished from narrow-band radio frequency interference. This effect will become progressively more serious for galaxies with smaller intrinsic velocity-widths. If, as we might expect, galaxies with smaller intrinsic velocity-widths have smaller HI masses, then compensating for this effect could significantly steepen the faint-end slope of the derived HIMF.

Key words: surveys – galaxies: evolution – galaxies: luminosity function, mass function – galaxies: distances and redshifts – large-scale structure of Universe.

1 INTRODUCTION

A complete and bias-free census of the population of extragalactic objects is essential to any study of the forma-

tion and evolution of galaxies or the large-scale structure of the universe. However, our current understanding of galaxy populations has been primarily derived from optical and IR

surveys. There is an inevitable bias in such surveys against low luminosity objects (dwarfs), but also against low surface brightness (LSB) objects (see, e.g. Disney 1976; Disney & Phillipps 1987; Impey & Bothun 1997; Disney 1999).

However, it has become clear that low luminosity and low surface brightness galaxies play a key role in many cosmological and cosmographical problems. For example, dwarf/LSB galaxies can clearly play a major role in helping us to understand large-scale structure and its influence on galaxy formation and evolution. Their numbers and distribution place constraints on the increasingly sophisticated numerical and semi-analytic models of galaxy formation (e.g., Baugh, Cole & Frenk 1996; Kauffmann et al. 1997), while their morphologies and stellar contents may reflect the local physics which define the star formation process in galaxies (e.g., Bell & Bower 2000; Bell & de Jong 2000).

Recent observational studies have fully supported the view (expounded by, e.g., Phillipps et al. 1987 and Impey, Bothun & Malin 1988) that low luminosity and low surface brightness galaxies numerically dominate the galaxy population in the local Universe (see e.g. McGaugh 1996; Cross et al. 2001). However, optical surveys of the local Universe for faint/LSB objects are problematic due to the very long exposure times required, the large areas which need to be surveyed and the need to measure a redshift for each faint/LSB object found. Consequently, our knowledge of the local population of galaxies at low luminosity and low surface brightness is still relatively limited. This inhibits our knowledge of many broader cosmological/cosmographical issues.

Given the limitations of optical surveys for detecting low luminosity / LSB objects, an alternative method to sample the extragalactic population is to use the 21-cm neutral hydrogen (HI) line. This provides a way of potentially circumventing optical selection effects operating against low luminosity and/or LSB objects, since a galaxy's HI content may be relatively uncorrelated with its optical emission. For example, it is well known that elliptical galaxies contain little HI whereas we might expect to find large amounts of HI in galaxies where star formation has been inefficient, e.g. in low luminosity and LSB galaxies. However, until comparatively recently, most HI surveys were limited to HI measurements of galaxies previously detected in optical or IR surveys. The advent of the 21-cm multibeam receiving systems at Parkes and Jodrell Bank has made possible, for the first time, blind HI surveys of large areas of sky to reasonable sensitivity over comparatively large volumes.

The HI Parkes All Sky Survey (HIPASS, Staveley-Smith et al. 1996) was commenced in 1997 and concluded in 2002. HIPASS has surveyed the southern hemisphere (up to $\delta=+25^\circ$) to $cz=12700 \text{ km s}^{-1}$ and an HI mass limit around $10^6 d_{\text{Mpc}}^2 M_\odot$. Results from HIPASS have indeed added significantly to the census of the local extragalactic population. Recent scientific highlights include the discovery of 10 new members to the Cen A group (Banks et al. 1999), the detection of an apparently extragalactic HI cloud with no optical counterpart to faint limits (Kilborn et al. 2000) and the discovery of a massive HI cloud associated with NGC 2442 (Ryder et al. 2001). Kilborn et al. (2002) have recently published a catalogue of 536 galaxies from a 2400 sq deg region of HIPASS covering the South Celestial Cap. Koribalski et al. (in preparation) will present the HIPASS Brightest Galaxies Catalogue (BGC), a catalogue of the brightest 1000 galaxies

(in terms of HI peak flux) from the whole of HIPASS. Meanwhile, Ryan-Weber et al. (2002) have discussed the properties of those previously uncatalogued galaxies found in the BGC.

The HI Jodrell All Sky Survey (HIJASS) is the northern counterpart to HIPASS. HIJASS will survey the northern sky above $\delta=22^\circ$ to similar sensitivity to HIPASS, using the Multibeam 4-beam cryogenic receiver mounted on the 76-m Lovell Telescope. HIJASS was begun in 2000. So far $\simeq 1115 \text{ deg}^2$ have been surveyed. We recently presented results from the HIJASS data covering the M81 group (Boyce et al. 2001). The survey reveals several new aspects to the complex morphology of the HI distribution in the group and illustrates that a blind HI survey of even such a nearby, well studied group of galaxies can add much new information.

This paper presents a detailed description of the HI Jodrell All Sky Survey and of the properties of the HI-selected sample of galaxies which has been compiled so far from the HIJASS data. We use the sample of confirmed HIJASS sources to study the effect that a galaxy's inclination to the line of sight has on its inclusion within an HI-selected sample. We show that both highly inclined galaxies and galaxies close to face-on are subject to selection effects which could have led to their being under-represented in previous determinations of the HI Mass Function (HIMF) and HI mass density, Ω_{HI} , from HI-selected samples of galaxies.

Section 2 describes the hardware, the observing strategy and survey parameters and also describes the data reduction methods. Section 3 describes the methods by which galaxies have been detected within HIJASS data and their parameters measured. Section 4 is a discussion of the properties of the sample of galaxies found in HIJASS data thus far. In Section 5 we use the sample of confirmed HIJASS sources to study the inclination-dependent selection effects on the inclusion of a galaxy in an HI-selected sample and discuss the implications of this. Section 6 presents some concluding remarks.

2 THE SURVEY

2.1 Hardware

HIJASS uses a cryogenic Multibeam receiver (Bird 1997) of similar design to the Multibeam receiver used at Parkes for HIPASS (Staveley-Smith et al. 1996). The Multibeam system installed at Jodrell Bank has four dual linearly polarised receivers covering a frequency range of 1200 MHz to 1550 MHz. The feed horn array consists of 4 stepped circular horns (which were designed at the CSIRO) arranged in a rhombic pattern, the apertures of which are located at the telescope prime focus. Stepped circular horns were chosen because of their good pattern symmetry, low spillover and good cross polarization properties (Bird 1994). The horns couple directly into a low temperature, high vacuum, cryogenic dewar. The output from the feed horn arrays are then fed to a set of 3-stage high electron mobility transistor (HEMT) pre-amplifiers which are cooled to a temperature of around $\sim 25 \text{ K}$. Following amplification, each receiver RF band is then down converted to an IF bandpass which can be set anywhere between 30 MHz and 245 MHz.

Each of the 8 resultant IF bands are then passed from

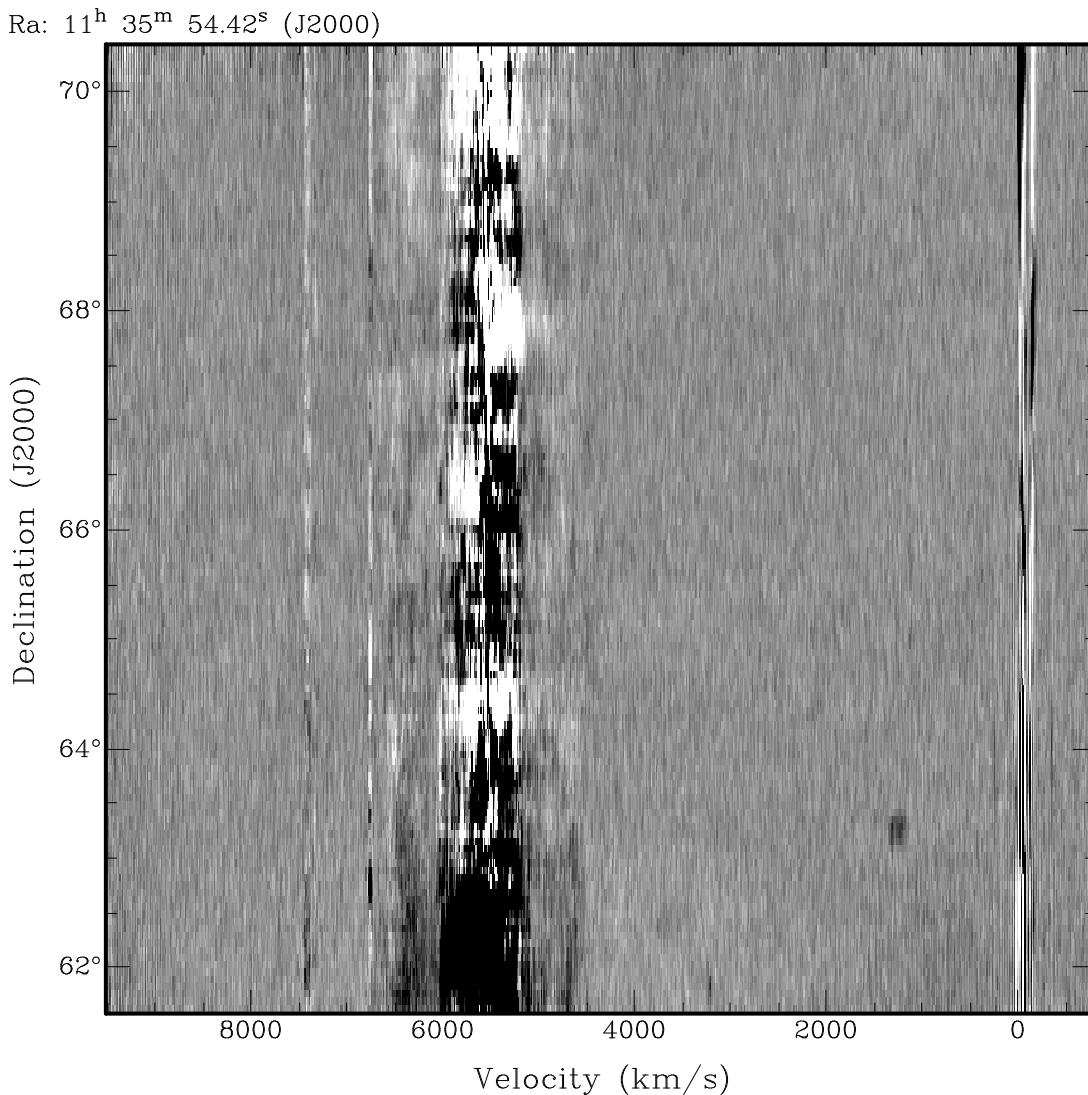


Figure 1. A section of a HIJASS cube at roughly constant *R.A.*. Visible are the residue of Galactic HI at 0 km s^{-1} , the galaxy UGC06534 at $V_{\odot} \simeq 1300 \text{ km s}^{-1}$; and the radio frequency interference between $4500 \rightarrow 7500 \text{ km s}^{-1}$.

the focus cabin to the observing room via about 300 m of low loss coaxial cable which is terminated into N-socket connections in the Lovell Observing Room. These outputs are next patched into a set of digitally programmable attenuators and are then fed into a set of equaliser and splitter units. Each IF is equalised for frequency dependent cable losses and then split into two outputs. The first output connects to a filter bank which sets the bandpass which is presented to the correlator. A second set of outputs are used for pulsar survey measurements.

The correlator was constructed at the Australia Telescope National Facility (ATNF). It is built around special purpose VLSI chips developed by the NASA Space Engineering Research Centre for VLSI System Design (Canaris 1993). These chips accept 2-bit sampled data streams at rates of up to 140 Msamples/sec and form either the cross correlation function of the two streams or the autocorrelation function of one stream at 1025 contiguous sample delays. The chip has 1024 32-bit accumulators and a 32-bit output bus and can integrate for up to 16 seconds. In the

multibeam correlator, one of these chips, operating in autocorrelation mode, is used on each of the 8 sampled data streams, thereby providing, after Fourier transformation, a measurement of the input spectrum at 1024 contiguous frequencies spaced at 62.5 kHz (equivalent to 13.2 km s^{-1} at the rest frequency of HI).

2.2 Observing strategy and data reduction

The survey is conducted by actively scanning the sky in 8° strips in Declination, at a rate of 1° per minute. Each declination scan is separated by 10 arcmin but each area of sky is scanned 8 times, resulting in a final scan separation of 1.25 arcmin. The data from the 8 correlators are stored every 5 s. A 64 MHz bandpass with 1024 channels is used, although local interference at the band edges restricts the useful velocity range to about -1000 km s^{-1} to $+10000 \text{ km s}^{-1}$ (note, however, that a broad band of radio frequency interference also affects all velocities between 4500 km s^{-1} and 7500 km s^{-1} - see Section 2.3). The sys-

Table 1. Areas surveyed by HIJASS

Decl. Range	R.A. Range	Area (deg ²)	Run
70°–78°	complete	795	2000,2001
62°–70°	09 ^h 02 ^m –11 ^h 55 ^m	128	2001,2002
	02 ^h 30 ^m –04 ^h 02 ^m	64	2002
54°–62°	03 ^h 26 ^m –04 ^h 08 ^m	32	2001
30°–38°	01 ^h 13 ^m –01 ^h 59 ^m	64	2002
22°–30°	12 ^h 08 ^m –12 ^h 34 ^m	32	2002

tem temperature is ~ 30 K. Bandpass correction and calibration are applied using the software package LIVEDATA (see Barnes et al. 2001). The spectra are gridded into three-dimensional $8^\circ \times 8^\circ$ datacubes (α, δ, V_\odot) using the software package GRIDZILLA (Barnes et al. 2001). The observed spectra are smoothed online by applying a 25 per cent Tukey filter to reduce ‘ringing’ caused by strong Galactic signals entering through the side-lobes. This reduces the actual velocity resolution in the gridded datacubes to 18.1 km s^{-1} . The spatial pixel size of the datacubes is $4 \text{ arcmin} \times 4 \text{ arcmin}$. The effects of continuum emission on the baselines of the spectra in each cube are then removed by the program POLYCON written by Daniel Zambonini and Robert Minchin. This program fits and then subtracts a 5th order polynomial baseline to each individual spectrum in a datacube: fitting is only performed on parts of the spectrum free of interference or line emission.

2.3 Areas Surveyed and Data Quality

HIJASS has been conducted during three observing runs: in April–June 2000; in Jan–Feb 2001; and in Jan 2002. Table 1 notes those areas of the northern sky so far surveyed by HIJASS and during which run the data were taken. The whole of a strip in R.A. between Decl.= $70^\circ \rightarrow 78^\circ$ has been surveyed (795 deg²). Two areas of the R.A. strip between Decl.= $62^\circ \rightarrow 70^\circ$ have also been surveyed (192 deg²), along with smaller areas at Decl.= 58° , 34° , and 26° . In total 1115 deg² has been surveyed thus far.

Fig. 1 shows an example of the data. This is a plot of Decl. against Velocity at roughly constant R.A.. The HIJASS source HIJASS J1133+63 can be seen at Decl. $\simeq 63^\circ$, $V_\odot = 1300 \text{ km s}^{-1}$. This has been identified as UGC 06534. Prominent in the data is a broad band of radio frequency interference (RFI) which affects all velocities from $\simeq 4500 \text{ km s}^{-1}$ to 7500 km s^{-1} . This is mainly due to off-site radio and data communication emissions generated in the locality.

Between the observing runs in 2001 and 2002, the Lovell dish underwent the first stage of a major upgrade. A new telescope drive system was installed and around half of the dish surface was replaced.

Prior to this upgrade, the rms noise in the datacubes (away from the broad-band RFI) was typically $16\text{--}18 \text{ mJy beam}^{-1}$. However, those cubes made from data taken following the first stage of the refurbishment (i.e. in 2002), show an improvement in sensitivity by around 25 per cent, the rms noise in these cubes being about $12\text{--}14 \text{ mJy beam}^{-1}$. The improvement is believed to be due to a combination of several factors: the improved sensitivity of the partially resurfaced dish, an improvement in the

telescope pointing model, an improvement in the smoothness of the scanning and a concerted effort to reduce local (Jodrell-based) interference during the observing run.

3 DETECTING AND PARAMETRIZING GALAXIES IN HIJASS DATA

3.1 Galaxy detection techniques

The general method of detecting galaxies in the HIJASS data is as follows. An initial candidate galaxy list is formed by visually searching the datacubes. The visual display program KVIEW (Gooch 1995) is used to search through the data in three dimensions by displaying 2 axes and stepping through the third. Narrow velocity-width, bright galaxies are most easily seen when the data are displayed in R.A. versus Decl. and stepped through Velocity. Broad velocity-width, faint galaxies are more easily discovered when the datacube is displayed R.A. or Decl. versus Velocity. The selection criteria for this visual sample is that a detection must: (1) be easily visible above the noise ($\sim 3\sigma$ in peak flux), (2) should have a spatial extent of greater than 1 pixel, and (3) be visible over two or more velocity planes. Two lists are compiled using these criteria: one of ‘definite’ detections and one of ‘possible’ detections. The list of possible detections includes sources close to the selection limit or just below it but still considered possible sources.

A second candidate galaxy list is formed by running the automated finding algorithm POLYFIND, written by Robert Minchin and Jonathon Davies. POLYFIND determines the noise in non-masked regions of a hanning smoothed datacube and then looks for peaks at some user-defined level above the noise (typically set at 3σ). It then runs a series of matched filters over these identified peaks and a peak is noted as a potential source if a sufficiently good fit is obtained. The results from POLYFIND are then re-checked by eye using the same criteria as used for the eyeball method and lists of definite and possible detections made.

The two lists of definite detections are then amalgamated and these objects included in our final sample of confirmed HIJASS galaxies. The two lists of possible detections are also amalgamated. These objects are then re-observed with the Lovell telescope in single-beam mode using a bandwidth of 16 MHz. Those possible sources confirmed by this narrow-band follow-up are then added to the sample of confirmed HIJASS sources. The possible sources found during the 2002 run have not yet been subjected to narrow-band follow-up. Hence, for the 2002 data, only the definite detections found by the above selection methods have presently been included in the sample (69 sources).

3.2 Parametrization of the galaxies

The parameters of those galaxies included in the sample of confirmed HIJASS sources are determined from the data using tasks from the MIRIAD software package (Sault et al. 1995). Firstly, a two-dimensional Gaussian fit (IMFIT) is made to a zeroth order (intensity) moment-map of each detection to determine the central position of the galaxy as well as the spatial extent of the HI. The central position

Table 2. The sample of confirmed HIJASS sources.

Source Name	R.A. (J2000)	Decl. (J2000)	S_{Int} Jy km s^{-1}	S_{Pk} mJy	rms mJy	V_o km s^{-1}	ΔV_{20} km s^{-1}	ΔV_{50} km s^{-1}	Class	Optical Counterpart	Position Offset (')	Velocity Offset (km s^{-1})
HIJ ASS J0002+77	00:02:31.1	77:17:43	9.53±0.99	61	11.8	2419	502	479	ID	UGC 12921	2.4	+30
HIJ ASS J0127+31	01:27:29.7	31:33:07	17.25±0.91	105	12.7	4040	363	332	ID	UGC 01033	1.2	-3
HIJ ASS J0133+30	01:33:23.9	30:43:09	780.66±0.86	7654	18.1	-175	146	103	ID	M33	6.8	-4
HIJ ASS J0149+32	01:49:30.5	32:34:57	32.94±0.72	281	14.8	150	153	121	ID	UGC 01281	0.4	+3
HIJ ASS J0253+64	02:53:45.3	64:06:01	17.62±0.77	169	15.6	3740	158	119	ASS	ZOAG G135.80+04.32	1.0	
HIJ ASS J0254+66	02:54:57.0	66:22:10	12.31±0.86	78	11.6	3456	390	374	ID*	MCG+11-04-003	2.1	-12
HIJ ASS J0258+75	02:58:48.2	75:45:29	27.04±0.92	143	13.5	2533	320	301	ID	UGC 02411	0.8	+14
HIJ ASS J0307+65	03:07:22.9	65:29:20	9.30±0.69	75	12.2	3532	217	192	ID	IRAS 03028+6516	2.1	+67
HIJ ASS J0308+62	03:08:00.5	62:10:16	9.00±0.68	89	12.6	3213	197	150	ID	[H92] 09	3.4	+7
HIJ ASS J0308+74	03:08:27.1	74:57:20	2.64±0.40	49	10.2	1462	90	76	PUG			
HIJ ASS J0308+65	03:08:44.3	65:00:38	6.58±0.77	109	18.4	529	105	70	PUG			
HIJ ASS J0309+65	03:09:01.1	65:39:12	17.13±0.89	120	14.5	2462	260	213	ID*	IRAS 03044+6528	1.8	-2
HIJ ASS J0310+74	03:10:26.8	74:13:27	4.17±0.63	58	11.5	2009	199	47	ID	kkh 019	3.7	+28
HIJ ASS J0312+67	03:12:35.0	67:25:10	10.65±0.69	67	11.0	3163	273	237	ID*	IRAS 03076+6712	2.6	-76
HIJ ASS J0315+64	03:15:16.6	64:52:44	22.62±0.80	244	15.7	2389	172	85	ID*	IRAS 03108+6441	0.7	-31
HIJ ASS J0316+67	03:16:42.2	67:12:43	11.50±0.60	119	12.0	2493	166	142	ASS	ZOAG G136.34+08.19	0.5	
HIJ ASS J0316+65	03:16:56.4	65:00:48	15.36±1.01	72	13.8	3167	378	322	ID*	IRAS 03123+6450	1.6	-22
HIJ ASS J0319+66	03:19:59.7	66:49:26	16.03±0.62	114	11.3	3005	200	185	ASS*			
HIJ ASS J0320+63	03:20:16.7	63:39:56	7.61±0.64	72	13.1	3267	157	148	ASS	ZOAG G138.56+05.39	0.9	
HIJ ASS J0321+54	03:21:17.7	54:56:13	8.59±1.10	152	30.5	1555	73	65	PUG			
HIJ ASS J0322+72	03:22:06.3	72:37:56	20.39±0.74	147	12.6	2591	241	218	ASS	2MASXi J0322123+723607	1.9	
HIJ ASS J0322+58	03:22:52.1	58:36:21	33.24±1.31	169	18.1	2314	370	297	ID*	IRAS 03189+5828	2.9	+6
HIJ ASS J0323+66	03:23:36.1	66:40:25	6.96±0.59	102	13.4	2171	119	72	PUG			
HIJ ASS J0325+67	03:25:49.4	67:53:43	3.55±0.43	46	9.3	1391	136	125	ASS	ZOAG G136.67+09.22	2.1	
HIJ ASS J0326+63	03:26:17.9	63:53:09	7.09±0.57	85	11.0	2008	180	158	ASS	ZOAG G138.98+05.94	1.8	
HIJ ASS J0326+68	03:26:55.0	68:35:02	24.14±0.70	178	11.5	1934	256	233	ID	UGC 02729	0.2	+6
HIJ ASS J0326+76	03:26:49.8	76:17:35	9.28±0.44	153	11.5	2125	84	58	ID	HFLLZOA G131.80+16.14	3.2	+6
HIJ ASS J0327+72	03:27:24.6	72:49:56	14.61±0.73	85	12.1	2080	247	234	ID	UGCA 069	2.3	-7
HIJ ASS J0327+67	03:27:58.2	67:07:40	41.43±0.62	518	13.4	1958	134	114	PUG			
HIJ ASS J0328+57	03:28:31.3	57:54:58	38.03±1.22	290	22.8	1427	192	177	PUG			
HIJ ASS J0329+64	03:29:17.5	64:58:38	13.17±0.80	75	10.0	2456	453	411	ASS*			
HIJ ASS J0330+55	03:30:51.0	55:57:22	30.59±0.84	326	17.5	1340	138	120	PUG			
HIJ ASS J0331+66	03:31:07.7	66:30:09	31.54±0.67	179	10.8	1603	262	241	ID*	IRAS 03266+6619	0.5	-23
HIJ ASS J0332+68	03:32:14.9	68:17:49	16.63±0.93	133	13.6	1730	327	105	ID	UGC 02765	4.4	-51
HIJ ASS J0332+66	03:32:22.9	66:08:36	7.68±0.42	114	10.5	1639	96	74	PUG			
HIJ ASS J0332+68	03:32:43.8	68:06:37	39.31±0.56	371	10.9	1347	175	109	ID	IRAS 03277+6755	1.3	-14
HIJ ASS J0335+75	03:35:01.4	75:09:23	4.21±0.56	59	12.9	2558	114	78	PUG			
HIJ ASS J0337+75	03:37:40.8	75:12:50	12.68±0.51	151	11.8	2501	113	99	ASS	HFLLZOA G133.03+15.74	2.4	
HIJ ASS J0337+72	03:37:51.1	72:33:57	18.71±0.62	173	13.0	2214	146	128	ID	NGC 1343	0.3	+1
HIJ ASS J0338+67	03:38:31.1	67:35:33	55.40±0.59	688	13.3	1439	122	92	ID	IRAS 03337+6725	0.3	-5
HIJ ASS J0339+71	03:39:45.3	71:23:45	22.66±0.62	169	13.0	1181	223	201	ID	UGC 02800	1.6	-5
HIJ ASS J0340+66	03:40:04.3	66:42:24	61.80±0.74	415	11.7	1502	273	256	ID	UGCA 081	0.4	-6
HIJ ASS J0347+70	03:47:19.6	70:10:07	26.15±0.70	182	15.0	1293	136	125	PUG			
HIJ ASS J0348+71	03:48:08.1	71:46:59	2.13±0.87	43	18.2	2547	147	135	PUG			
HIJ ASS J0348+68	03:48:22.5	68:16:20	408.99±0.57	11129	17.7	97	51	32	PUG			

Table 2. Continued.

Source Name	R. A. (J2000)	Decl. (J2000)	S_{Int} Jy km s^{-1}	S_{Pk} mJy	rms mJy	V_o km s^{-1}	ΔV_{20} km s^{-1}	ΔV_{50} km s^{-1}	Class	Optical Counterpart	Position Offset (')	Velocity Offset (km s^{-1})
HIJASS J0348+70	03:48:23.7	70:07:56	90.78±1.13	328	14.2	1178	451	371	ID	UGC 02855	0.1	+24
HIJASS J0350+70	03:50:11.6	70:06:11	51.53±1.53	198	18.7	1283	482	231	ID*	UGC 02866	0.6	-51
HIJASS J0352+65	03:52:06.5	65:11:02	8.87±0.73	94	15.2	1266	148	137	PUG			
HIJASS J0352+74	03:52:54.4	74:09:33	8.57±0.60	101	12.9	2555	137	85	ASS*			
HIJASS J0355+67	03:55:08.1	67:55:28	4.82±0.48	87	12.2	1279	90	49	PUG			
HIJASS J0355+70	03:55:57.8	70:16:57	6.06±0.84	75	17.9	1376	142	99	ASS	HFLZOA G137.35+12.75	1.9	
HIJASS J0357+72	03:57:37.4	72:48:01	3.86±0.83	61	17.2	1150	149	85	PUG			
HIJASS J0357+66	03:57:38.2	66:07:07	7.79±0.72	72	12.2	3448	240	193	PUG			
HIJASS J0358+69	03:58:19.7	69:16:41	5.91±0.59	82	13.2	1302	127	105	ID	BK19	0.6	0
HIJASS J0400+67	04:00:13.1	67:09:07	332.80±0.41	4654	21.9	65	156	66	ID	UGCA 086	2.3	+1
HIJASS J0401+56	04:01:06.2	56:25:30	1.74±0.73	55	21.1	3564	66	56	PUG			
HIJASS J0402+71	04:02:32.0	71:41:10	10.52±0.52	86	20.2	4573	230	199	ID	UGC 02916	1.2	-56
HIJASS J0402+71	04:02:57.2	71:42:30	17.89±0.94	169	20.2	4451	220	198	ID	CGCG 327-013	0.8	-58
HIJASS J0403+74	04:03:08.2	74:11:22	9.28±0.51	265	16.4	2574	47	31	ASS	HFLZOA G135.05+16.10	4.0	
HIJASS J0404+71	04:04:07.4	71:31:57	3.93±0.62	65	13.8	1725	128	113	ID	BK21	4.7	+9
HIJASS J0407+69	04:07:36.7	69:45:45	101.78±2.40	360	13.8	886	479	460	ID	IC 0356	3.1	+9
HIJASS J0409+70	04:09:04.6	70:25:36	8.23±1.15	78	20.7	736	206	188	ASS*			
HIJASS J0423+75	04:23:11.7	75:17:31	33.03±1.05	238	15.3	2475	329	300	ID	NGC 1530	1.0	-14
HIJASS J0430+71	04:30:17.5	71:42:56	1.89±0.58	61	16.8	3124	64	29	PUG			
HIJASS J0443+75	04:43:43.6	75:36:22	16.97±0.81	102	12.7	2476	281	263	ID	NGC 1530A	3.4	0
HIJASS J0445+72	04:45:47.3	72:46:53	10.96±1.61	97	23.2	4798	339	308	ID	UGC 03131	3.0	-44
HIJASS J0445+76	04:45:58.7	76:24:36	41.04±0.90	241	15.1	989	242	230	ID	UGC 03137	1.2	+3
HIJASS J0447+74	04:47:24.1	74:56:55	18.02±0.77	160	15.8	1639	154	132	ID	UGC 03144	2.3	-3
HIJASS J0509+73	05:09:47.1	73:21:03	4.60±0.44	121	13.4	1266	56	39	PUG			
HIJASS J0520+76	05:20:31.5	76:21:17	15.52±0.88	88	12.8	2483	332	245	ID	UGC 03276	2.7	+20
HIJASS J0529+72	05:29:32.1	72:23:49	7.67±0.51	151	14.3	1106	70	52	ID	[HS98] OD	3.7	-17
HIJASS J0533+73	05:33:25.9	73:42:18	13.32±0.56	139	12.3	1238	129	109	ID	UGC 03317	1.5	+2
HIJASS J0545+73	05:45:19.9	73:36:41	4.70±0.53	68	11.8	1053	127	83	ID*	KUG 0539+735	1.1	+46
HIJASS J0545+72	05:45:26.1	72:22:07	10.18±0.45	78	8.2	1080	199	163	ID	UGC 03343	0.7	+10
HIJASS J0556+75	05:56:28.7	75:18:40	23.70±0.88	228	18.4	811	146	129	ID	UGC 03371	0.7	+5
HIJASS J0602+73	06:02:25.1	73:04:46	18.31±0.56	224	12.8	1095	119	77	ID	UGC 03384	4.1	-6
HIJASS J0610+71	06:10:23.0	71:23:17	16.02±0.70	87	11.3	1270	268	231	ID	UGC 03403	1.1	-6
HIJASS J0615+71	06:15:24.5	71:06:29	8.87±0.28	56	14.9	3981	325	220	ID	UGC 03422	2.2	-60
HIJASS J0619+75	06:19:15.8	75:01:14	1.75±0.42	41	10.9	1324	85	75	ASS	2MASX J0620153+745817	4.8	
HIJASS J0655+69	06:55:49.8	69:39:03	6.72±0.95	120	16.4	1196	290	56	ID	UGC 03580	5.5	+5
HIJASS J0711+71	07:11:32.4	71:49:40	21.51±0.83	99	12.2	3144	321	298	ID	UGC 03697	0.9	-7
HIJASS J0713+73	07:13:28.8	73:29:30	10.47±0.64	105	12.2	2702	183	122	ID	UGC 03730 (Pair)	3.8	+5
HIJASS J0716+75	07:16:10.9	75:43:42	9.72±0.45	138	11.1	1118	96	79	ID	UGC 03739	1.5	+2
HIJASS J0721+74	07:21:20.9	74:18:45	1.45±0.53	61	14.3	966	77	44	PUG			
HIJASS J0722+77	07:22:12.5	77:49:01	7.11±0.57	67	11.1	2643	172	156	ID	UGC 03794	2.1	+13
HIJASS J0730+72	07:30:35.1	72:29:29	12.28±0.88	108	15.3	2620	223	175	ID*	UGC 03864 (Group)	2.3	-51
HIJASS J0736+74	07:36:12.5	74:25:10	6.61±0.55	70	9.6	3776	221	119	ID*	UGC 03906 (Pair)	2.6	-72
HIJASS J0736+73	07:36:39.4	73:41:59	13.52±0.59	111	11.1	943	188	170	ID	UGC 03909	1.5	+2
HIJASS J0744+72	07:44:58.4	72:47:54	10.14±0.58	201	15.3	2476	83	59	ID	UGC 03975	0.8	+4
HIJASS J0750+74	07:50:14.4	74:19:57	14.56±0.94	84	14.3	3943	298	180	ID	UGC 04028	2.8	+9

Table 2. Continued.

Source Name	R.A. (J2000)	Decl. (J2000)	S_{Int} Jy km s ⁻¹	S_{Pk} mJy	rms mJy	V_o km s ⁻¹	ΔV_{20} km s ⁻¹	ΔV_{50} km s ⁻¹	Class	Optical Counterpart	Position Offset (')	Velocity Offset (km s ⁻¹)
HIJASS J0751+72	07:51:46.1	72:59:37	10.62±1.11	119	22.7	3470	156	104	ID	NGC 2441	1.5	0
HIJASS J0752+74	07:52:11.6	74:35:11	6.71±0.59	56	10.9	2346	196	156	ASS	KUG 0746+747	3.1	
HIJASS J0752+72	07:52:54.5	72:03:04	5.40±0.19	59	10.0	2483	111	81	ID*	UGC 04050	0.7	+16
HIJASS J0755+78	07:55:34.9	78:00:50	9.10±0.56	123	13.1	2294	114	90	ID	NGC 2336A	2.1	+2
HIJASS J0811+76	08:11:26.6	76:23:25	22.39±0.57	149	10.8	1538	187	170	ID	UGC 04238	2.0	+6
HIJASS J0818+70	08:18:39.7	70:42:01	195.86±0.60	3588	16.5	156	74	54	ID	Holmberg II	2.3	+1
HIJASS J0824+71	08:24:01.9	71:00:36	3.62±0.54	83	15.9	117	62	42	ID	M81DWARFA	1.3	-4
HIJASS J0824+74	08:24:41.2	74:24:06	8.79±0.82	135	14.7	3532	93	67	ID	UGC 04363	2.4	-3
HIJASS J0827+73	08:27:29.4	73:28:31	19.35±0.86	131	15.9	2169	195	166	ID	UGC 04390	3.0	0
HIJASS J0828+73	08:28:07.5	73:41:01	9.62±0.77	99	14.1	3677	200	100	ID	NGC 2550A	4.5	-36
HIJASS J0836+69	08:36:47.6	69:43:54	8.71±0.85	280	27.7	157	44	30	ID	UGC 04483	2.9	+21
HIJASS J0837+77	08:37:51.4	77:59:01	15.00±0.43	95	12.8	1335	299	263	ID	NGC 2591	2.9	-13
HIJASS J0848+73	08:48:07.9	73:31:15	16.90±0.75	116	13.4	2374	210	157	ID	IC 2389	1.3	+7
HIJASS J0848+74	08:48:23.9	74:02:01	23.47±0.82	128	10.8	2111	402	232	ID	NGC 2633	4.1	+49
HIJASS J0908+78	09:08:18.9	78:04:01	39.53±0.81	186	12.3	1317	302	281	ID	NGC 2715	1.3	+22
HIJASS J0913+76	09:13:18.6	76:27:09	30.88±0.83	146	12.1	1494	324	278	ID*	NGC 2748	2.0	-18
HIJASS J0915+74	09:15:05.4	74:13:51	21.90±0.66	172	12.3	1126	193	161	ID	Holmberg III	1.2	+1
HIJASS J0918+73	09:18:28.1	73:44:08	20.74±0.71	109	10.6	2263	313	296	ID	IC 0529	1.5	-1
HIJASS J0920+64	09:20:23.4	64:05:57	90.07±0.68	1129	15.9	1740	114	90	ID	NGC 2805	0.4	-10
HIJASS J0922+75	09:22:07.9	75:44:32	2.87±0.39	85	11.4	660	60	27	ID	UGC04945	1.8	-1
HIJASS J0928+66	09:28:51.9	66:28:16	8.19±0.59	91	13.3	3438	124	107	ID	UGC 05042	1.6	-3
HIJASS J0932+76	09:32:00.0	76:26:58	10.84±0.88	82	15.2	2175	238	144	ID*	UGC 05050	3.1	+2
HIJASS J0938+76	09:38:44.2	76:18:05	19.79±0.53	134	9.3	2286	217	203	ID	NGC 2938	1.6	-1
HIJASS J0940+71	09:40:34.3	71:12:00	34.21±0.61	1086	19.5	140	48	30	ID	Holmberg I	1.1	+3
HIJASS J0947+67	09:47:46.8	67:55:50	58.20±0.69	439	13.4	-40	172	100	ID	NGC 2976	3.1	+37
HIJASS J0950+67	09:50:19.9	67:06:31	10.96±0.91	91	15.4	3920	239	176	ID*	KUG 0946+674	4.0	-7
HIJASS J0950+72	09:50:33.1	72:16:00	79.25±1.05	433	15.5	1315	322	302	ID	NGC 2985	1.1	+7
HIJASS J0951+65	09:51:52.1	65:28:32	10.80±0.46	229	13.0	3362	69	37	ID	UGC 05277	1.6	+3
HIJASS J0955+69	09:55:18.6	69:07:16	326.19±0.99	2816	17.6	-40	459	388	ID	M81	3.6	+6
HIJASS J0955+69	09:55:27.2	69:40:18	149.38±1.78	1116	32.2	184	204	132	ID	M82	2.2	+19
HIJASS J0956+72	09:56:01.6	72:11:09	71.87±0.81	460	14.2	1052	223	208	ID	NGC 3027	1.9	+6
HIJASS J0956+75	09:56:43.7	75:50:05	14.79±0.85	96	13.6	2461	272	189	ID	NGC 3061	2.7	-4
HIJASS J0957+69	09:57:19.0	69:05:40	24.00±7.20	600	32.2	59	75	40	ID*	Holmberg IX	3.1	+6
HIJASS J0957+69	09:57:22.4	69:19:41	35.04±9.51	730	32.2	99	57	48	ASS	A0952+69	2.8	
HIJASS J0957+68	09:57:55.5	68:39:02	35.60±7.12	1780	17.6	-151	80	50	ID	KDG061	5.9	+16
HIJASS J1002+72	10:02:16.6	72:05:39	5.82±0.76	66	14.7	2109	177	81	ID	NGC 3066	1.9	-60
HIJASS J1003+68	10:03:49.1	68:42:19	173.65±0.72	3353	17.9	9	93	35	ID	NGC 3077	3.1	+5
HIJASS J1005+70	10:05:22.4	70:20:24	3.14±0.66	74	17.4	335	84	58	ID	UGC 05423	1.6	+15
HIJASS J1015+65	10:15:09.3	65:08:43	16.23±1.00	116	15.4	3321	293	237	ID	UGC 05520	1.0	-6
HIJASS J1017+73	10:17:28.4	73:23:55	22.97±0.95	98	12.6	2794	403	366	ID	NGC 3147	2.5	+26
HIJASS J1018+74	10:18:00.0	74:20:40	11.54±0.79	74	12.1	2940	296	255	ID	NGC 3155	1.4	+4
HIJASS J1021+68	10:20:31.0	68:42:00	8.64±0.41	303	12.9	43	57	37	PUG			
HIJASS J1022+74	10:22:01.0	74:10:07	19.94±0.92	100	12.8	3098	364	304	ID	NGC 3183	0.9	-10
HIJASS J1022+77	10:22:12.8	77:54:43	2.03±0.58	53	12.3	1671	143	90	PUG			
HIJASS J1023+70	10:23:52.4	70:52:52	13.82±0.77	124	15.1	1013	171	147	ID	UGC 05612	1.2	-2

Table 2. Continued.

Source Name	R.A. (J2000)	Decl. (J2000)	S_{Int} Jy km s^{-1}	S_{Pk} mJy	rms mJy	V_o km s^{-1}	ΔV_{20} km s^{-1}	ΔV_{50} km s^{-1}	Class	Optical Counterpart	Position Offset (')	Velocity Offset (km s^{-1})
HIJASS J1028+66	10:28:16.7	66:43:37	4.51±0.55	58	11.0	1130	166	127	ID	UGC 05671	5.9	+6
HIJASS J1029+68	10:29:08.5	68:26:23	187.07±0.63	2600	14.0	64	126	104	ID	IC 2574	4.7	-7
HIJASS J1030+70	10:30:06.8	70:02:49	11.09±0.45	202	12.6	1917	72	54	ID	UGC 05688	1.6	+3
HIJASS J1032+77	10:32:33.5	77:51:19	1.96±0.44	56	12.3	1633	72	30	ID	UGC 05701	3.3	-9
HIJASS J1032+65	10:32:37.1	65:01:44	35.74±1.03	198	16.8	1670	256	235	ID	NGC 3259	0.8	+16
HIJASS J1034+73	10:34:01.2	73:44:08	9.18±0.98	72	15.2	1140	290	99	ID	NGC 3252	2.3	+16
HIJASS J1046+63	10:46:36.6	63:13:21	146.19±0.66	775	10.7	1019	261	238	ID	NGC 3359	0.1	-5
HIJASS J1048+72	10:48:28.8	72:24:38	9.08±0.66	94	12.0	2731	201	159	ID	NGC 3364	0.9	0
HIJASS J1049+65	10:49:13.8	65:31:34	12.74±0.44	201	11.8	341	83	66	ID	UGC 05918	2.4	-1
HIJASS J1052+67	10:52:44.7	67:58:50	7.24±0.48	96	11.5	1111	108	89	ID	UGC 05979	0.6	+5
HIJASS J1053+73	10:53:47.9	73:41:28	40.62±0.93	275	14.1	1268	301	281	ID	NGC 3403	0.5	-6
HIJASS J1112+65	11:12:13.8	65:14:34	2.81±0.50	54	11.1	1051	128	92	ID	UGC 06237	1.1	+17
HIJASS J1120+67	11:20:11.9	67:14:55	10.51±0.52	93	10.5	1316	159	143	ID	NGC 3622	0.4	-10
HIJASS J1121+69	11:21:59.9	69:37:18	12.30±0.54	106	10.2	1317	184	145	ID	UGC 06378	1.0	-11
HIJASS J1122+64	11:22:32.9	64:03:45	10.03±0.73	89	14.3	1011	172	160	ID	UGC 06390	1.0	+4
HIJASS J1125+63	11:25:24.3	63:43:12	12.59±0.58	198	15.5	3729	80	59	ID	UGC 06429	0.8	-3
HIJASS J1126+64	11:26:36.6	64:05:14	3.51±0.54	60	13.9	981	89	79	ID	UGC 06448	3.4	+6
HIJASS J1133+61	11:33:18.6	61:49:36	3.84±0.47	102	13.5	3273	64	28	ID	UGC 06528	4.1	-23
HIJASS J1133+63	11:33:31.6	63:17:25	19.36±0.91	167	16.3	1272	212	135	ID	UGC 06534	1.4	+1
HIJASS J1134+71	11:34:23.3	71:30:54	9.78±0.72	62	11.5	2821	273	194	ID*	UGC 06552	1.7	-14
HIJASS J1142+77	11:42:52.2	77:21:34	5.80±0.52	53	9.7	1683	195	177	ID	NGC 3901	0.9	+3
HIJASS J1144+69	11:44:36.4	69:45:55	7.07±0.58	72	10.8	2709	194	136	ID	UGC 06711	2.2	-7
HIJASS J1146+69	11:46:52.1	69:22:07	15.00±0.66	108	11.5	1441	221	199	ID	NGC 3879	0.9	-10
HIJASS J1147+69	11:47:38.1	69:09:58	7.86±0.58	63	10.2	1465	214	156	ID	UGC 06764	3.7	-4
HIJASS J1205+77	12:05:18.3	77:29:25	11.22±0.60	77	8.7	2023	336	274	ID	UGC 07086	2.2	-15
HIJASS J1208+76	12:08:30.9	76:48:52	20.91±0.64	162	10.2	1828	272	242	ID	NGC 4127	0.7	-11
HIJASS J1208+29	12:08:37.7	29:12:44	21.23±1.62	130	21.1	3884	419	318	ASS*			
HIJASS J1209+25	12:09:43.2	25:00:02	10.77±0.76	94	13.1	2570	227	208	ID	UGC 07143	1.7	+3
HIJASS J1209+29	12:09:07.5	29:56:49	35.58±1.40	449	33.2	610	108	88	ID	NGC 4136	2.5	-1
HIJASS J1211+76	12:11:19.5	76:06:19	9.02±0.69	121	12.1	1752	219	165	ID*	NGC 4159	2.0	-16
HIJASS J1211+24	12:11:56.6	24:06:21	13.91±0.79	81	11.4	2563	333	320	ID	NGC 4162	1.4	+6
HIJASS J1212+29	12:12:13.7	29:07:34	5.59±0.44	87	11.0	3998	93	65	ID*	NGC 4174	3.2	-18
HIJASS J1212+29	12:12:21.0	29:12:00	35.92±0.70	310	13.4	1113	179	161	ASS*			
HIJASS J1213+24	12:13:54.9	24:15:03	4.09±0.37	81	10.3	950	72	61	ID	UGC 07236	1.6	-5
HIJASS J1213+75	12:13:52.2	75:04:31	5.49±0.61	62	9.6	2272	280	129	ID	UGC 07226	3.3	0
HIJASS J1213+28	12:13:21.6	28:33:07	12.67±0.84	82	11.6	3896	374	337	ID	NGC 4185	2.5	+8
HIJASS J1216+30	12:16:36.2	30:20:30	4.46±0.41	67	10.4	3830	91	74	ASS	MAP-NGP 0-321-0285578	0.8	
HIJASS J1216+28	12:16:44.1	28:43:55	11.62±0.40	192	10.3	1215	89	70	ID	UGC 07300	0.2	-5
HIJASS J1217+22	12:17:24.6	22:31:42	31.43±0.68	229	11.6	420	235	214	ID	UGC 07321	2.2	-12
HIJASS J1217+70	12:17:49.8	70:48:33	8.81±0.54	126	11.6	2048	143	122	ID	NGC 4250	2.0	-19
HIJASS J1219+28	12:19:22.6	28:21:29	7.84±0.61	57	10.1	2527	251	222	ASS*			
HIJASS J1222+26	12:22:12.1	26:04:04	3.22±0.36	38	7.9	1019	134	112	ID	IC 3215	1.0	0
HIJASS J1222+76	12:22:55.6	76:08:14	11.00±0.72	104	11.7	1581	257	157	ID	NGC 4331	2.4	-12
HIJASS J1224+74	12:24:07.9	74:59:16	7.38±0.55	59	10.2	1411	197	178	ID*	NGC 4363	3.3	+16
HIJASS J1225+26	12:25:18.4	26:43:11	13.06±0.54	100	10.4	321	180	134	ID	IC 3308	0.3	-5

Table 2. Continued.

Source Name	R.A. (J2000)	Decl. (J2000)	S_{Int} Jy km s ⁻¹	S_{Pk} mJy	rms mJy	V_o km s ⁻¹	ΔV_{20} km s ⁻¹	ΔV_{50} km s ⁻¹	Class	Optical Counterpart	Position Offset (')	Velocity Offset (km s ⁻¹)
HIJ ASS J1225+27	12:25:51.5	27:34:01	35.69±0.50	359	10.7	743	138	118	ID	NGC 4393	0.3	+12
HIJ ASS J1225+28	12:25:13.0	28:23:41	5.99±0.60	86	13.3	4510	128	115	ID	IC 3309	1.8	+5
HIJ ASS J1225+28	12:25:32.7	28:29:58	6.44±0.50	124	13.3	481	79	44	ID	LEDA 166137	1.3	+5
HIJ ASS J1228+28	12:28:24.3	28:40:16	7.51±0.78	65	12.9	4458	247	197	ID	UGC 07597	0.5	0
HIJ ASS J1228+22	12:28:41.1	22:49:06	29.63±0.56	249	11.6	642	152	134	ID	NGC 4455	0.7	-5
HIJ ASS J1231+29	12:31:59.4	29:42:02	8.16±0.46	134	12.1	642	84	68	ID	UGC 07673	0.6	0
HIJ ASS J1233+24	12:33:46.5	24:00:37	3.60±0.52	65	15.0	1329	65	24	ASS*			
HIJ ASS J1242+75	12:42:08.8	75:15:31	4.38±0.51	59	10.9	1896	137	72	ID	UGC 07872	3.1	-18
HIJ ASS J1246+71	12:46:56.4	71:10:37	15.27±0.85	88	13.0	1665	299	256	ID	NGC 4693	1.0	+5
HIJ ASS J1250+72	12:50:18.9	72:51:52	10.41±0.86	69	12.7	1628	321	265	ID	NGC 4750	1.1	-5
HIJ ASS J1255+74	12:55:38.2	74:24:54	2.61±0.54	35	10.5	3164	176	166	PUG			
HIJ ASS J1300+73	13:00:14.0	73:40:47	6.87±0.67	51	10.9	1650	260	197	ID	UGC 08120	1.5	+15
HIJ ASS J1315+73	13:15:12.7	73:06:52	1.94±0.49	47	13.0	2837	83	76	PUG			
HIJ ASS J1321+75	13:21:17.8	75:20:13	2.02±0.94	84	29.3	2533	52	44	PUG			
HIJ ASS J1323+70	13:23:14.4	70:30:46	9.53±0.75	72	14.6	3097	176	146	ID	NGC 5144 (Pair)	1.7	+38
HIJ ASS J1632+78	16:32:55.3	78:12:45	50.07±0.84	339	15.0	1354	211	183	ID	NGC 6217	1.2	+8
HIJ ASS J1643+70	16:43:41.2	70:46:01	11.80±0.86	102	16.0	1284	191	169	ID	NGC 6236	4.5	-4
HIJ ASS J1646+70	16:46:18.2	70:21:03	30.76±0.84	257	16.5	1132	171	150	ID	NGC 6248	0.5	-3
HIJ ASS J1710+72	17:10:25.6	72:21:55	18.44±0.91	125	14.4	1192	276	176	ID	IC 1251	2.8	-24
HIJ ASS J1711+72	17:11:51.8	72:05:53	3.25±0.58	51	11.4	1307	168	84	ASS	87GB 171345.8+720715	5.3	
HIJ ASS J1714+75	17:14:12.5	75:11:51	7.08±0.38	149	10.5	1234	71	54	ID	UGC 10792	0.8	-1
HIJ ASS J1720+71	17:20:40.7	71:32:11	2.38±0.37	65	10.2	2495	70	33	PUG			
HIJ ASS J1726+71	17:26:44.5	71:06:18	10.55±0.65	89	11.2	1156	230	195	ID	NGC 6395	1.2	+8
HIJ ASS J1729+74	17:29:26.0	74:17:26	5.98±0.42	63	9.0	1904	214	166	ID	UGC 10892	2.5	+23
HIJ ASS J1729+75	17:29:46.8	75:42:45	19.59±0.55	171	12.1	1318	141	117	ID	NGC 6412	0.8	+6
HIJ ASS J1729+77	17:29:52.2	77:21:44	3.74±0.56	59	10.1	1828	209	154	ID*	UGC 10907	2.1	-6
HIJ ASS J1736+72	17:36:45.7	72:05:45	12.15±0.78	61	11.3	2491	340	305	ID	NGC 6434	0.5	-8
HIJ ASS J1819+74	18:19:57.5	74:35:59	27.53±1.04	154	14.7	1491	353	335	ID	NGC 6643	1.9	-7
HIJ ASS J1834+70	18:34:41.8	70:30:04	29.22±0.75	214	13.2	495	217	190	ID	NGC 6689	1.5	+5
HIJ ASS J2012+74	20:12:06.5	74:15:59	2.34±0.46	54	12.6	2330	74	45	PUG			
HIJ ASS J2016+75	20:16:45.4	75:07:32	6.67±0.21	64	11.2	1844	186	132	PUG			
HIJ ASS J2147+72	21:47:00.0	72:27:43	25.92±0.74	168	11.4	2404	289	254	ID	UGC 11818	1.3	-2
HIJ ASS J2151+71	21:51:08.1	71:12:11	10.67±0.69	94	13.8	2537	160	130	PUG			
HIJ ASS J2155+73	21:55:29.9	73:14:55	40.53±0.80	215	12.9	1485	266	245	ID	UGC 11861	4.0	-4
HIJ ASS J2201+71	22:01:07.5	71:55:16	13.87±0.77	79	12.0	2540	285	269	ID*	IRAS 22002+7142	1.5	-42
HIJ ASS J2229+75	22:29:22.6	75:22:10	25.70±1.00	143	15.4	2461	295	275	ID*	IRAS 22282+7506	0.5	-16
HIJ ASS J2230+76	22:30:30.2	76:30:57	10.28±0.74	99	14.6	2366	167	156	ID	UGC 12069	1.0	+1
HIJ ASS J2241+75	22:41:18.5	75:09:56	26.80±1.08	172	17.7	1549	254	237	ID	UGC 12160	1.6	+6
HIJ ASS J2245+73	22:45:43.1	73:08:25	7.82±0.98	90	17.9	1538	201	115	ID*	UGC 12182	1.4	-4
HIJ ASS J2253+75	22:53:46.0	75:15:12	8.66±0.51	94	10.7	1662	147	130	ASS	UGC 12247	1.0	
HIJ ASS J2256+71	22:56:19.3	71:33:05	3.66±0.45	74	12.2	1540	75	39	ID	UGC 12261	4.5	+3
HIJ ASS J2257+72	22:57:03.5	72:44:02	25.30±0.83	200	13.8	2668	246	223	ID	UGC 12263	1.5	+8

is then used to generate a spatially integrated spectrum of the detection, using a box size based on the extent of the HI. The spectrum is generated using MBSPECT which also gives a measurement of the peak and integrated flux of each detection, as well as the 50 per cent and 20 per cent velocity-width, the rms noise and barycentric velocity.

Table 2 presents the derived parameters for the sample of confirmed HIJASS sources. Column 1 gives the HIJASS Name. Columns 2 and 3 give the Right Ascension (J2000) and Declination (J2000) from the IMFIT task. Columns 4-6 list the zeroth order moment (Integrated flux $S_{\text{int}} = \int S_V dV$), the peak flux (S_{peak}), and the noise (rms dispersion around the baseline, σ); all as measured by MBSPECT. Columns 7-9 give the first order moment (barycentric velocity V_{\odot}), the velocity width at 20 per cent of the peak flux (ΔV_{20}), and the velocity width at 50 per cent of the peak flux (ΔV_{50}), all measured by MBSPECT in the radio frame and converted to *cz*. The error in integrated flux is calculated from the rms noise on the spectrum and the velocity extent of the source.

Columns 10-13 contain the details of any counterpart to the HIJASS source, as listed in the NASA/IPAC Extragalactic Database (NED). Column 10 contains one of five possible classifications. If there is no object within NED which could be spatially coincident with the HIJASS source (defined as being within 6 arcmin), then Column 10 contains the classification ‘PUG’ (i.e. Previously Uncatalogued Galaxy). If there is an object in NED which matches the HIJASS source in both position and space (defined as being within 6 arcmin and 100 km s^{-1}) then this is listed as ‘ID’ (Identification). Those IDs which have been detected in HI for the first time by HIJASS are denoted by an asterisk, i.e. ‘ID*’. If there is an object within NED which is spatially coincident with the HIJASS source (i.e. within 6 arcmin) but for which no redshift is listed in NED, then Column 10 contains the classification ‘ASS’ (i.e. Association). In several cases, there is more than one galaxy within 6 arcmin: in these cases the classification ‘ASS*’ is used. For the ID, ID* and ASS classifications, Column 11 lists the object within NED which appears to correspond to the HI detection. Column 12 lists the position offset (in arcmin) of the coordinates of the optical counterpart from the HI position. Column 13 lists (for the IDs and ID*s) the velocity offset of the barycentric velocity contained within NED from the barycentric velocity as measured by HIJASS.

4 PROPERTIES OF THE HIJASS GALAXIES

4.1 Composition of the sample

There are currently 222 sources included in the sample of confirmed HIJASS sources. Of these, 170 (77 per cent) are clearly associated with a previously catalogued galaxy (classification ID or ID*). However, 25 of these 170 objects have been detected in HI for the first time by HIJASS (classification ID*). For 4 of these 170 sources, HIJASS appears to be measuring HI from a pair or a small group of galaxies which lie at the redshift of the HI.

There are a further 23 HIJASS sources (10 per cent of the whole sample) which lie within 6 arcmin of a catalogued galaxy for which no redshift is reported in NED (classification ASS or ASS*). These HIJASS sources may or may

not be associated with the catalogued galaxy. 15 of these sources have only one possible optical counterpart within 6 arcmin of the HI position (classification ASS). We may be relatively confident about the optical identification of these sources. However, even for these sources there remains the possibility that the HI has been detected from an associated HI cloud (cf. Ryder et al. 2001) or a LSB companion. The other 8 of the 23 sources have more than one galaxy within 6 arcmin of the HIJASS position (classification ASS*). We intend to obtain accurate positions for all 23 of these sources using HI aperture synthesis observations, so as to unambiguously determine the optical counterpart of each source.

There are then a further 29 sources (13 per cent of the whole sample) which do not lie within 6 arcmin of any previously catalogued galaxy (classification PUG). A study of the Digital Sky Survey (DSS) at the positions of these sources reveals an obvious and unambiguous optical counterpart in only 5 cases (J0327+67, J0721+74, J1720+71, J2016+75 and J2151+71). Fig. 2 presents the DSS images of these five PUGs. Three of these objects (J0327+67, J2016+75, J2151+71) have a compact but relatively high surface brightness core but a low surface brightness disk. They may have been excluded from optical catalogues because they were mistaken for stars. One object (J0721+74) is a highly inclined but relatively high surface brightness object, although very small ($\simeq 1$ arcmin diameter). The fifth object (J1720+71) has a complex morphology and appears to be involved in some kind of interaction or merger.

A study of the DSS for the other 24 PUGs, reveals no unambiguous optical counterpart. In many cases there are several possible optical candidates within the positional uncertainty of HIJASS. In several cases, however, no possible candidate can be seen. The optical counterparts of these sources must be of very low surface brightness. All of the PUGs will have accurate positions determined from aperture synthesis observations and will be the subject of deep optical follow-up work.

It is interesting to compare the number of PUGs found in the sample of confirmed HIJASS sources with those found in the Bright Galaxy Catalogue (BGC: Koribalski et al., in preparation). The BGC contains the 1000 brightest (in HI peak flux) sources in the whole of the HIPASS sample. 87 of these objects had not been previously catalogued, although 57 of these lie close (within 10°) to the Galactic plane. Of the other 30 previously uncatalogued galaxies within the BGC, Ryan-Weber et al. (2002) found a single optical counterpart for 25 on the DSS. Whilst the relative number of previously uncatalogued galaxies within the BGC is much smaller than within the HIJASS sample (3 per cent compared to 13 per cent), most of the BGC objects can be unambiguously assigned to an optical counterpart on the DSS, whilst most of the HIJASS PUGs cannot be. These differences are probably primarily due to the different flux limits of the two samples. The faintest source in the BGC has a peak flux of 116 mJy. Only 6 of the 29 HIJASS PUGs have a peak flux larger than this. The much lower peak flux limit of HIJASS has produced a much larger fraction of PUGs compared to the BGC. Since these have generally lower HI flux, they are correspondingly harder to detect in optical data.

As it currently stands, the sample of confirmed HIJASS sources presents the first HI measurement of 77 galaxies (i.e. classes ID*, ASS, ASS*, PUG), 35 per cent of the whole sam-

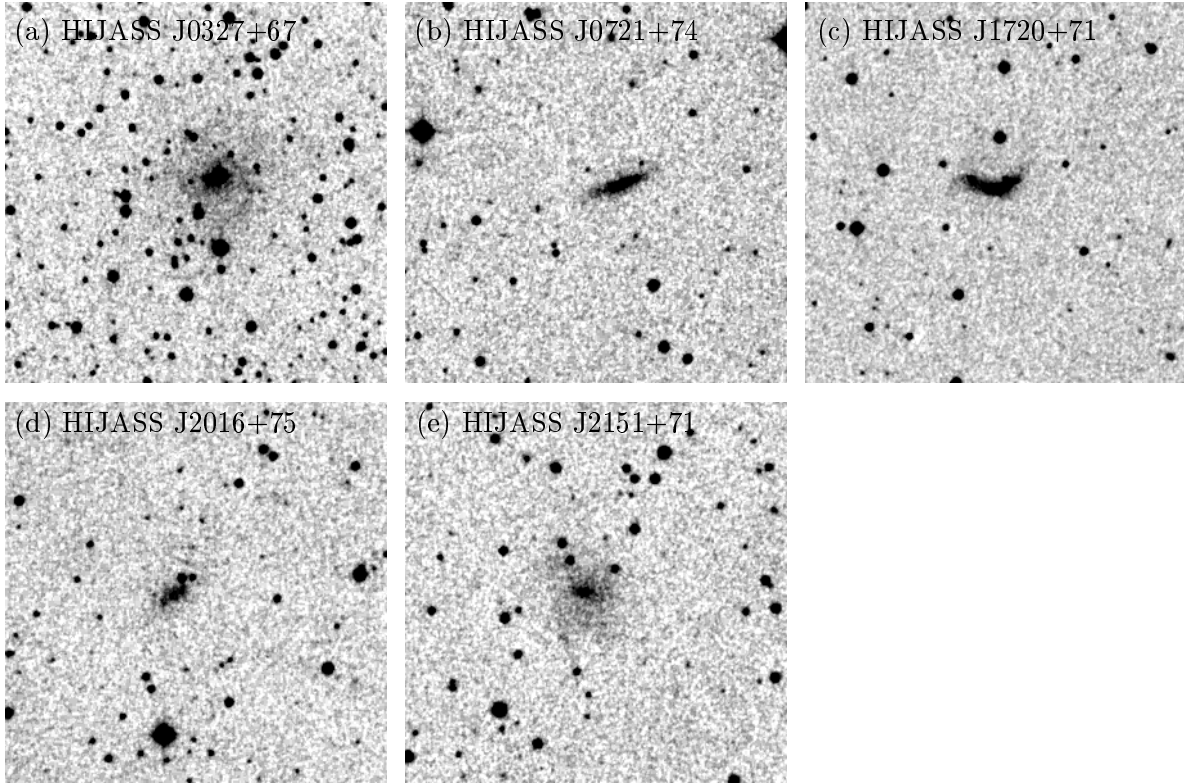


Figure 2. Digital Sky Survey images of the 5 PUGs for which an obvious and unambiguous optical counterpart can be seen. Each image is 5 arcmin \times 5 arcmin.

ple. It presents the first redshift measurement of 52 galaxies (i.e. classes ASS, ASS*, PUG), 23 per cent of the whole sample. Between 29 and 52 (13 and 23 per cent) of the objects within it have not been previously catalogued. It must also be noted that the ‘possible’ detections from the 2002 observing run have not yet been followed up. Based on the results of previous narrow-band follow-up, this will probably lead to an additional 5-10 sources being added to the sample, many of them previously uncatalogued sources.

4.2 Peak and integrated flux distributions

The main factor which determines the inclusion of a galaxy within the HIJASS sample ought to be its peak flux (rather than integrated flux). Eyeball searches are inevitably drawn to sources with larger peak fluxes. The POLYFIND automated finding algorithm also initially looks for peaks in individual pixels. Fig. 3 is a histogram of the peak flux of every source in the sample of confirmed HIJASS sources. For a peak flux limited survey of a homogeneous distribution of galaxies we expect $N_{\text{obj}} \propto S_{\text{Pk}}^{-5/2}$. The curve on Fig. 3 shows the best fit of this function to the observed distribution. This implies that our sample is complete to $S_{\text{Pk}} \simeq 80$ mJy. We noted above that the rms noise in HIJASS data shows considerable variation between cubes. In particular, the cubes from the 2002 run have considerably lower noise. The completeness limit of 80 mJy corresponds to a 5σ detection in the pre-upgrade data. The 3σ detection limit for the post-upgrade data is at $\simeq 39$ mJy. Only 2 sources have a peak flux less than this.

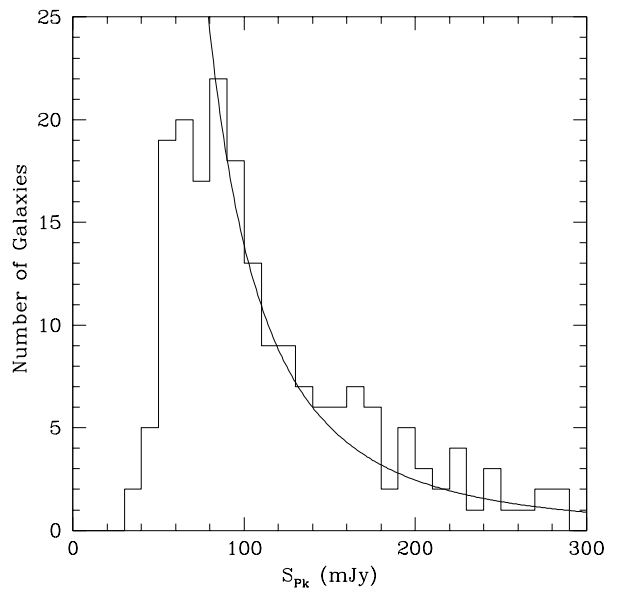


Figure 3. Peak flux distribution of HIJASS sources. The curve shows the best-fit to the data of the function $N_{\text{obj}} \propto S_{\text{Pk}}^{-5/2}$, i.e. that expected for a peak flux limited sample of a homogeneous distribution of galaxies.

Fig. 4 is a plot of S_{Pk} against 20% velocity-width (ΔV_{20}). Marked on this is the peak flux detection limit at $S_{\text{Pk}}=39$ mJy (3σ for the post-upgrade data). This figure also shows another important selection effect in our sam-

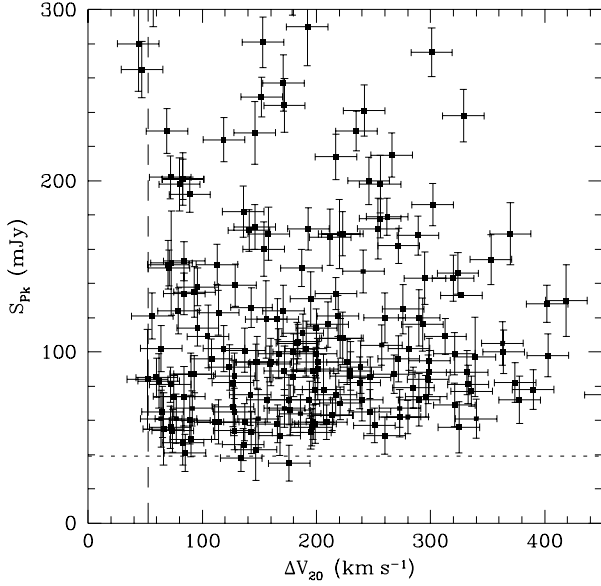


Figure 4. Plot of S_{Pk} against ΔV_{20} for the sample of confirmed HIJASS sources. The short-dashed line shows the 3σ peak flux detection limit for the post-upgrade data at 39 mJy. The long-dashed line shows the velocity-width limit equivalent to 4 channels, $\Delta V_{20}^{\text{lim}}=52.8 \text{ km s}^{-1}$.

ple: we detect few galaxies at $\Delta V_{20} < 50 \text{ km s}^{-1}$. This is because there is a minimum believable velocity-width which a galaxy must have in order to be selected as a real source from our data. Sources with a narrower velocity-width will be mistaken for narrow band radio frequency interference. From the data it appears that this minimum believable velocity-width is around 4 channels wide for ΔV_{20} , i.e. $\Delta V_{20}^{\text{lim}}=52.8 \text{ km s}^{-1}$. This makes intuitive sense as it allows 2 ‘high’ channels where the source is seen and believed and 2 ‘low’ channels where the flux is dropping off down to the 20 per cent level. The locus of this limit is drawn on Fig. 4 and constrains the data well. In Section 5 we consider the implications of this velocity-width limit for the completeness of HI-selected samples of galaxies.

Because the HIJASS sample is approximately peak flux limited, the detection of a galaxy of a given integrated flux, S_{Int} , will (even in similar noise) be a function of its velocity-width: broader velocity-width galaxies of a given integrated flux have a lower peak flux and therefore are less likely to be detected than a narrower galaxy of the same integrated flux. This is clearly seen in Fig. 5, a plot of $\log(S_{\text{Int}})$ against ΔV_{20} . From this can be seen a clear trend for the minimum detected integrated flux to increase with increasing velocity-width.

For a given profile shape we expect the integrated flux, S_{Int} , 20% velocity-width, ΔV_{20} , and the peak flux, S_{Pk} , to be related via

$$S_{\text{Int}} = k \Delta V_{20} S_{\text{Pk}} \quad (1)$$

where k is a constant which depends on the profile shape. For a top-hat function $k \approx 1$, for a Gaussian $k \approx 0.7$. Fig. 6 is a plot of S_{Int} against $\Delta V_{20} \cdot S_{\text{Pk}}$ for all galaxies in the HIJASS sample. The linearity of this relationship is clear although there is some expected scatter in the value of k . A

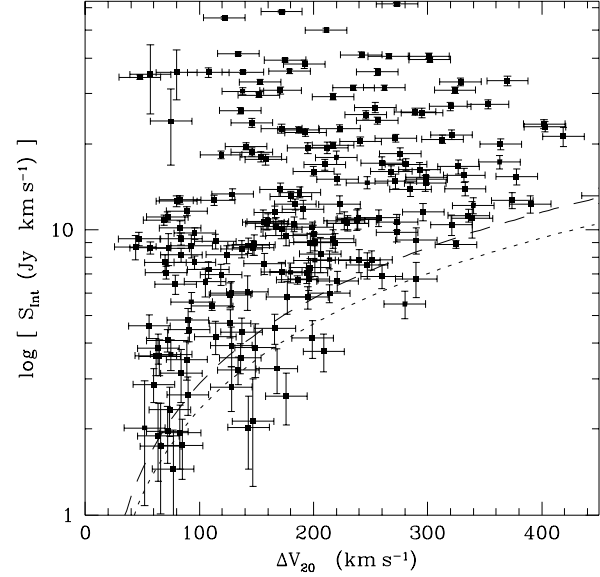


Figure 5. Plot of $\log(S_{\text{Int}})$ against ΔV_{20} for all the galaxies in the HIJASS sample. The long-dashed line is the locus of equation (3) for $S_{\text{Pk}}^{\text{lim}}=48 \text{ mJy}$ (i.e. a 3σ detection from the pre-upgrade observing runs). The short-dashed line is the locus of equation (3) for $S_{\text{Pk}}^{\text{lim}}=39 \text{ mJy}$ (i.e. a 3σ detection from the post-upgrade observing run).

least-squares best-fit to this data produces a mean value of $k \approx 0.6$. Adopting this value we can say

$$S_{\text{Int}} \approx 0.6 \Delta V_{20} S_{\text{Pk}} \quad (2)$$

for the HIJASS sample. Hence, for a given peak flux limit, $S_{\text{Pk}}^{\text{lim}}$, the integrated flux limit, $S_{\text{Int}}^{\text{lim}}$ is a function of ΔV_{20} via:

$$S_{\text{Int}}^{\text{lim}} \approx 0.6 \Delta V_{20} S_{\text{Pk}}^{\text{lim}} \quad (3)$$

The loci of this relationship for $S_{\text{Pk}}^{\text{lim}}=48 \text{ mJy}$ (i.e. a 3σ detection from the pre-upgrade observing runs) and for $S_{\text{Pk}}^{\text{lim}}=39 \text{ mJy}$ (i.e. a 3σ detection from the post-upgrade observing run) are plotted on Fig. 5. These describe well the form of the observed cut-off in S_{Int} as a function of ΔV_{20} .

It is worth noting that the fact that our sample is essentially peak flux limited has a dramatic effect on the proportion of broad velocity-width to narrow velocity-width galaxies included in the sample, compared to the proportion we would expect to find in an integrated flux limited sample. For the sake of illustration, we consider the fraction of galaxies with $S_{\text{Int}} > 3 \text{ Jy km s}^{-1}$ which will be included in the HIJASS sample as a function of velocity-width. The value of 3 Jy km s^{-1} corresponds to a galaxy of velocity-width 100 km s^{-1} with a peak flux of about 48 mJy (the 3σ limit for the pre-upgrade data). At $\Delta V_{20}=100 \text{ km s}^{-1}$, all galaxies with $S_{\text{Int}} > 3 \text{ Jy km s}^{-1}$ will be included in the HIJASS sample. However, at broader velocity-widths, the integrated flux limit will increase [equation (3)] and the sample will contain a progressively smaller fraction of galaxies with $S_{\text{Int}} > 3 \text{ Jy km s}^{-1}$.

In Table 3 we list (Column 2) the $S_{\text{Int}}^{\text{lim}}$ values equivalent to a range of ΔV_{20} values (Column 1) using equation (3) and assuming $S_{\text{Pk}}=48 \text{ mJy}$. For each pair of ΔV_{20} , $S_{\text{Int}}^{\text{lim}}$ values we list (Column 3) the fraction of galaxies with $S_{\text{Int}} > 3 \text{ Jy km s}^{-1}$ which will be missing from the HIJASS

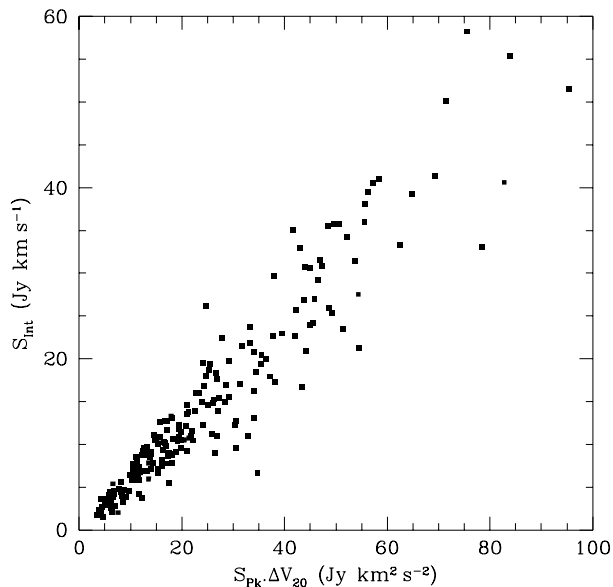


Figure 6. Plot of S_{Int} against $\Delta V_{20} S_{\text{Pk}}$ for the galaxies in the sample of confirmed HIJASS sources.

Table 3. The fraction of galaxies with $S_{\text{Int}} > 3 \text{ Jy km s}^{-1}$ which will be missed from the HIJASS sample as a function of ΔV_{20} . This assumes $S_{\text{Pk}}^{\text{lim}} = 48 \text{ mJy}$ and that the distribution of galaxies in space at each ΔV_{20} is homogeneous.

ΔV_{20} km s^{-1}	$S_{\text{Pk}}^{\text{lim}}$ Jy km s^{-1}	frac of gals missed
150	4.32	0.42
200	5.76	0.62
250	7.20	0.73
300	8.64	0.80
350	10.08	0.84
400	11.52	0.87

sample. This has been calculated assuming a homogeneous distribution of sources with $N_{\text{obj}} \propto S_{\text{Int}}^{-5/2}$ at each ΔV_{20} .

At $\Delta V_{20} = 150 \text{ km s}^{-1}$ only 68 per cent of galaxies with $S_{\text{Int}} > 3 \text{ Jy km s}^{-1}$ will be included in the HIJASS sample. At $\Delta V_{20} > 300 \text{ km s}^{-1}$ less than 20 per cent of galaxies with $S_{\text{Int}} > 3 \text{ Jy km s}^{-1}$ will be included. This is a particularly important selection effect since we might reasonably expect that broader velocity-width galaxies will tend to have higher HI masses (see e.g. Rao & Briggs 1993). Hence, compared to an integrated flux limited sample, our selection techniques may be significantly biased against the inclusion of higher HI mass galaxies. This effect will not bias an HIMF derived from the data provided that the selection effect is properly accounted for. It does, however, mean that the morphological mix of galaxies revealed by a blind HI survey is going to be biased towards narrow velocity-width dwarf galaxies and away from broad velocity-width giant galaxies. This bias needs to be born in mind when considering the relative proportions of the different morphologies of galaxies in an HI-selected sample.

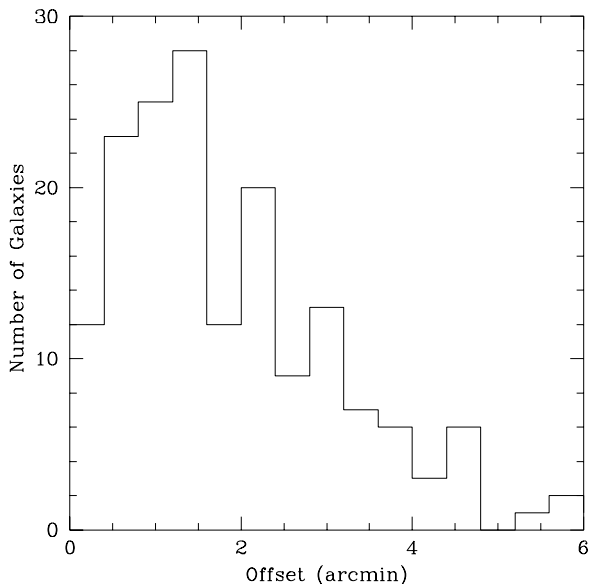


Figure 7. Histogram showing the distribution of the offset between HIJASS source position and the position of the identified optical counterpart.

4.3 Positional accuracy of HIJASS

The positional accuracy of HIJASS sources can be judged by considering the offset between the HIJASS positions and the positions listed in NED for those galaxies identified as being associated with each HIJASS source (i.e. the IDs and ID*s). Fig. 7 shows a histogram of these offsets. The majority of HIJASS sources (71 per cent) lie within 2.5 arcmin of the NED position, with only a very small fraction (7 per cent) lying beyond 4 arcmin.

4.4 Mass distribution

Fig. 8(a) shows a histogram of the distribution of HI masses for the whole of the sample of confirmed HIJASS sources. Galaxies within the M81 group have been assumed to lie at 3.63 Mpc (Freedman et al. 1994). The distances of the other galaxies have been determined from their redshifts (assuming $H_0 = 75 \text{ km s}^{-1} \text{ Mpc}^{-1}$). There is a peak in this distribution at $\sim 10^{9.6} M_{\odot}$. This is close to the value found for M_{HI}^* of $10^{9.75} M_{\odot}$ by Zwaan et al. (1997).

Although the HIJASS bandpass stretches to 10000 km s^{-1} , the RFI problem beyond $cz = 4500 \text{ km s}^{-1}$ effectively places a bandpass limit at this point. A galaxy with an HI mass of $10^{9.75} M_{\odot}$ would have an integrated flux of about 6.6 Jy km s^{-1} at this $cz = 4500 \text{ km s}^{-1}$. This is similar to the limiting integrated flux one would expect for a broad velocity-width ($\gtrsim 200 \text{ km s}^{-1}$) galaxy. Hence, HIJASS is effectively bandpass-limited for galaxies with $M_{\text{HI}} \gtrsim M_{\text{HI}}^*$ (assuming Zwaan et al.'s value for M_{HI}^*). For galaxies with $M_{\text{HI}} \lesssim M_{\text{HI}}^*$, HIJASS is flux limited.

Fig. 8(b) shows the HI mass distribution only for those 77 galaxies which had not previously been detected in HI (i.e. classes ID*, ASS, ASS* and PUG). This distribution is very similar to that of the whole sample. In fact, most of those 25 previously catalogued galaxies which had not previously been detected in HI, have HI masses be-

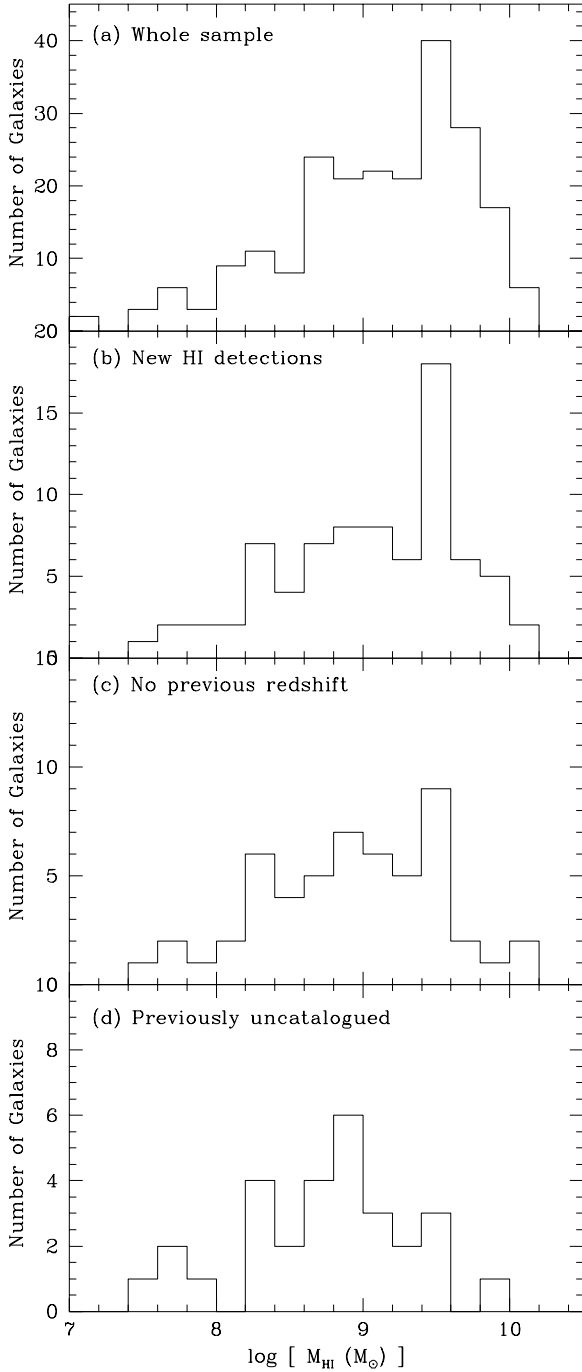


Figure 8. (a) M_{HI} distribution of the whole of the HIJASS sample; (b) M_{HI} distribution of the 77 galaxies which had not previously been detected in HI (classes ID*, ASS, ASS*, PUG); (c) M_{HI} distribution of the 52 galaxies with no previous redshift measurement (classes ASS, ASS*, PUG); (d) M_{HI} distribution for the 29 PUGs.

tween $10^{9.3}$ – $10^{9.8}$ M_{\odot} . All but 2 have integrated fluxes above 10 Jy km s^{-1} . These would appear to mostly be ‘normal’ galaxies which had simply not been observed in HI prior to HIJASS.

Fig. 8(c) shows the HI mass distribution for the 52 HIJASS objects which had no previous redshift measurement (classes ASS, ASS*, PUG). The peak at $10^{9.5}$ M_{\odot} is

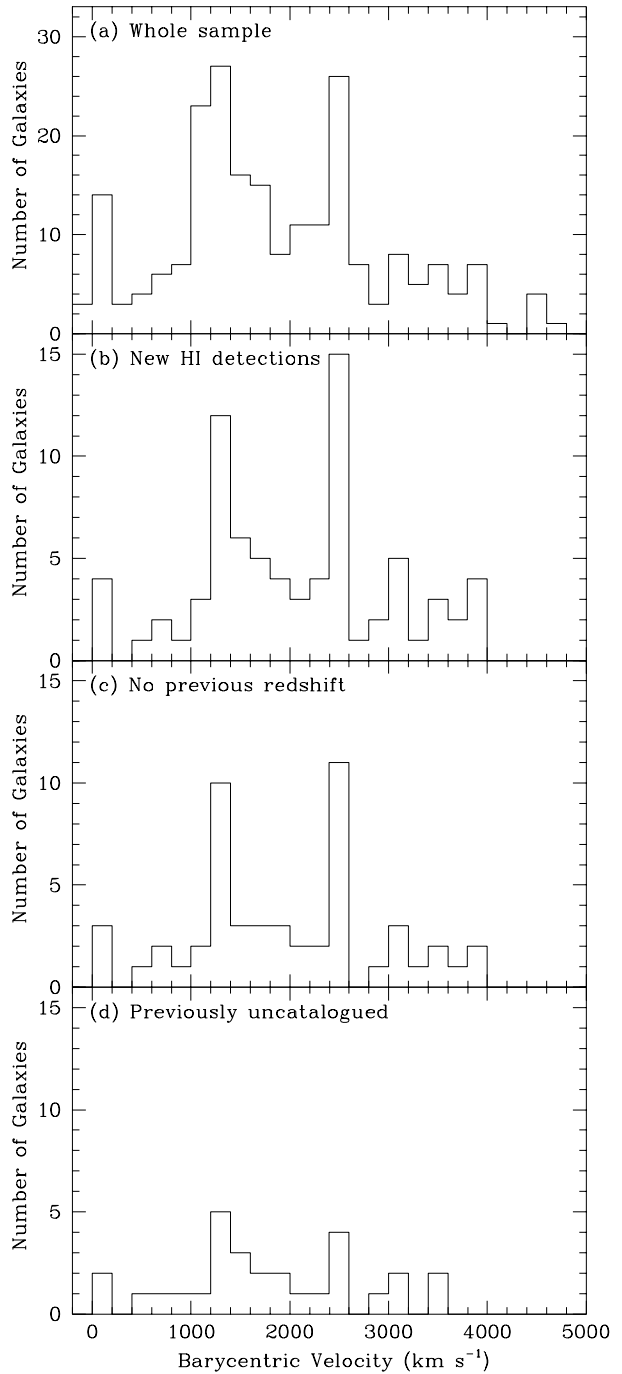


Figure 9. (a) The cz distribution of the whole of the HIJASS sample; (b) the cz distribution of the 77 galaxies which had not previously been detected in HI (classes ID*, ASS, ASS*, PUG); (c) the cz distribution of the 52 galaxies with no previous redshift measurement (classes ASS, ASS*, PUG); (d) the cz distribution for the 29 PUGs.

much less pronounced in this plot. A weaker peak in this distribution can be seen at $10^{8.9}$ M_{\odot} . A peak at this mass is clearly seen in Fig. 8(d) which plots the HI mass distribution for the 29 PUGs. The peak in this distribution is at about $10^{8.9}$ M_{\odot} , an order of magnitude below the peak in the distribution for the whole sample. In fact 69 per cent of the PUGs lie at $M_{\text{HI}} < 10^9$ M_{\odot} . In comparison only 39

per cent of the full sample lie in this mass range. A similar result was found by Ryan-Weber et al. (2002) for the 30 previously uncatalogued galaxies in the BGC at $|b| > 10^\circ$. They found the mass distribution of these 30 galaxies to peak at $10^{8.7} M_\odot$, compared to a peak at $10^{9.5} M_\odot$ for the whole of the BGC. This tendency for the newly discovered galaxies to have lower HI masses suggests a correlation between HI mass and optical detectability.

4.5 Velocity distribution

Fig. 9(a) shows the distribution of all the HIJASS galaxies as a function of cz . The peak close to 0 km s^{-1} is due to galaxies in the Local Group and the M81 Group. Beyond that there are prominent peaks at $cz \sim 1200 \text{ km s}^{-1}$ and 2500 km s^{-1} . These are due to large-scale structure. Note that only a handful of galaxies have been identified beyond 4500 km s^{-1} . This is mainly due to the increasing problems of RFI beyond this point and the difficulty of distinguishing any galaxies from interference.

Fig. 9(b) shows the cz distribution for all of those 77 galaxies which had not previously been detected in HI (Classes ID*, ASS, ASS*, PUG). This distribution is very similar to that of the whole sample. Fig. 9(c) shows the cz distribution for the 52 objects which had no previous redshift measurement (classes ASS, ASS*, PUG). Fig. 9(d) plots the HI mass distribution just for the 29 PUGs. All of these distributions show the same peaks at $cz = 1200 \text{ km s}^{-1}$ and 2500 km s^{-1} as that seen in Fig 8(a). Clearly, the distribution of new HI detections, new redshift measurements and newly catalogued galaxies follows that of the large-scale structure as revealed by the whole sample. This is particularly interesting in regard to the previously uncatalogued galaxies. These have a HI mass distribution with a peak an order of magnitude lower than that of the whole sample (see Fig. 8(d)) but the cz distribution is not skewed to nearer distances.

The relationship of HIJASS galaxies to large-scale structure is further explored in Fig. 10. This is a diagram showing the relationship of HIJASS galaxies (filled triangles) and all objects with redshifts in NED (open circles) in the complete *R.A.* strip between *Decl.* = $70^\circ \rightarrow 78^\circ$. The general association of HIJASS sources with the large-scale structure as delineated by the NED objects is clear. Most of those previously uncatalogued objects found by HIJASS lie in regions already populated with galaxies. Some of the structures which can be seen in the data include the group of galaxies at *R.A.* $\sim 17^h$, $V_\odot \sim 1200 \text{ km s}^{-1}$ (which includes NGC 6217, NGC 6236, NGC 6248 and NGC 6395); the NGC 4291 group at *R.A.* $\sim 13^h$, $V_\odot \sim 1600 \text{ km s}^{-1}$; a group including UGC 03317, UGC 03343 and UGC 03403 at *R.A.* $\sim 6^h$, $V_\odot \sim 1200 \text{ km s}^{-1}$; and two prominent ‘walls’, at *R.A.* $\sim 3^h \rightarrow 5^h$, $V_\odot \sim 2600 \text{ km s}^{-1}$ and at *R.A.* $\sim 7^h \rightarrow 10^h$, $V_\odot \sim 2300 \text{ km s}^{-1}$.

We have thus far failed to positively detect any galaxy beyond $cz = 4800 \text{ km s}^{-1}$. The presence of RFI between $cz = 4500\text{--}7500 \text{ km s}^{-1}$ makes the detection of galaxies in the region practically impossible. None the less, the band between $7500\text{--}9000 \text{ km s}^{-1}$ is generally free from RFI and we ought to be able to detect any galaxies in this region. However, to be detectable beyond $cz = 7500 \text{ km s}^{-1}$, a galaxy would need an HI mass of $\gtrsim 10^{10.9} M_\odot$. Such objects must

be very rare. For example, Kilborn et al.’s (2002) survey of 2400 deg^2 of HIPASS data did not detect any galaxy this massive. Minchin (2001) presented results from surveying a 32 deg^2 with the Parkes multibeam system to $12\times$ the standard HIPASS exposure time. No galaxy with $M_{\text{HI}} > 10^{10.6} M_\odot$ was detected.

4.6 Comparison to HIPASS

Following the first stage of the Lovell telescope upgrade, the rms noise in HIJASS data is around $12\text{--}14 \text{ mJy beam}^{-1}$. The typical noise in HIPASS data is $\sim 14 \text{ mJy beam}^{-1}$, although there is considerable variation between HIPASS cubes with rms spanning the range $9\text{--}17 \text{ mJy beam}^{-1}$.

The data at *R.A.* $\sim 12^h 08^m \rightarrow 12^h 34^m$, *Decl.* = $22^\circ \rightarrow 30^\circ$, observed during the 2002 run, was taken specifically because it provides a small overlap with the HIPASS survey between *Decl.* = $22^\circ \rightarrow 25^\circ$. Fig. 11 shows the integrated fluxes from HIPASS and HIJASS cubes for those galaxies which lie in the overlap region. The calibration between the surveys appears robust.

As noted in Section 4.4, terrestrial-based RFI effectively limits the HIJASS bandpass to $cz < 4500 \text{ km s}^{-1}$ whereas HIPASS can survey out to 12700 km s^{-1} . However, only galaxies with $M_{\text{HI}} \gtrsim M_{\text{HI}}^*$ can be seen beyond 4500 km s^{-1} in HIPASS data. In fact less than 24 per cent of the HIPASS sample presented by Kilborn et al. (2002) lies beyond 4500 km s^{-1} . HIPASS therefore, has an advantage over HIJASS in that very massive sources can be detected over larger volumes. However, for galaxies with $M_{\text{HI}} \lesssim M_{\text{HI}}^*$, both HIJASS and HIPASS are flux limited and HIJASS is potentially more sensitive.

5 INCLINATION-DEPENDENT SELECTION EFFECTS IN AN HI-SELECTED SAMPLE

The distribution function of neutral hydrogen masses among galaxies and intergalactic clouds (the HI mass function, HIMF) and, more generally, the neutral hydrogen density in the local Universe, Ω_{HI} , are important inputs into models of cosmology and galaxy evolution. Prior to the advent of blind HI surveys, astronomers were restricted to constructing an HIMF by making HI measurements of optically selected samples of galaxies (see, e.g. Rao & Briggs 1993; Solanes, Giovanelli & Haynes 1996).

In recent years several authors have attempted to determine the HIMF of the local Universe using an HI-selected sample of galaxies, with conflicting results. For example, using the data from the the Arecibo HI Strip Survey (Sorar 1994), Zwaan et al. (1997) derived an HIMF with a shallow faint end slope ($\alpha = 1.2$) consistent with earlier HIMFs derived from optically selected samples. In contrast the HIMF derived from the Arecibo Slice survey (Schneider, Spitzak & Rosenberg 1998; Spitzak & Schnedier 1998) has an upturn in its lowest mass bin, although this is due to only 2 galaxies in this bin. Recently, Rosenberg & Schneider (2002) have also reported a steep faint end slope ($\alpha \approx 1.5$) to the HIMF they have derived from the Arecibo Dual-Beam Survey (Rosenberg & Schneider 2000). HIPASS and HIJASS will provide much larger samples of galaxies and greatly improve the statistics of such determinations of the HIMF.

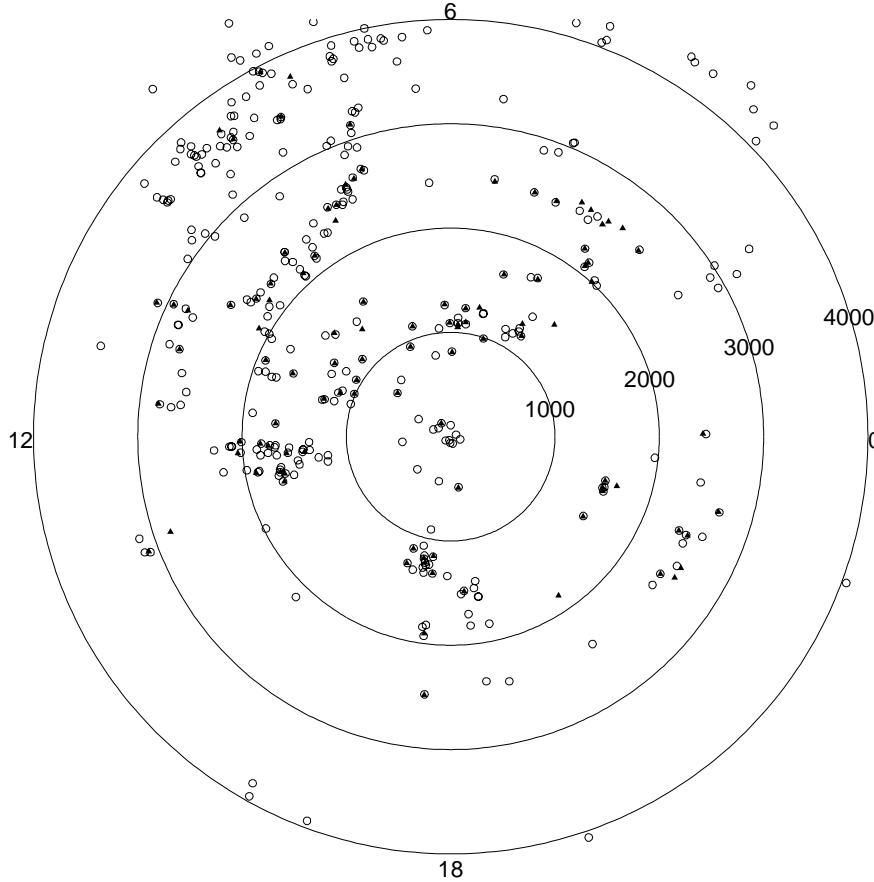


Figure 10. Distribution of R.A. vs cz of HIJASS galaxies in the range Decl.= $70^\circ \rightarrow 78^\circ$ (filled triangles). Also shown (open circles) is the R.A. vs cz distribution of all galaxies within NED within this declination range and with measured redshifts.

However, previous studies based upon HI-selected samples of galaxies have tended to overlook the important effect that the inclination of a galaxy to the line of sight could have on its inclusion in such a sample. There are two factors to be considered.

Firstly, highly inclined galaxies may suffer from significant self-absorption. Studies of the HI emission from galaxies have generally assumed that the HI line is optically thin in all circumstances. Relatively few authors (e.g. Epstein 1964a,b; Haynes & Giovanelli 1984) have addressed the issue of whether the HI emission from galaxies is actually optically thin in all galaxies. If this assumption is not valid for highly inclined galaxies, then the HI masses of such galaxies will have been underestimated. Some highly inclined galaxies will be missed altogether from an HI-selected sample of galaxies, despite less inclined galaxies of the same HI mass being included. Both of these effects will lead to errors in the derived HIMF.

Secondly, as noted in Section 4.2, there is a minimum believable velocity-width, $\Delta V_{20}^{\text{lim}}$, which an object in a blind HI survey must have in order to be distinguishable from narrow-band radio frequency interference. For any given type of galaxy, the measured velocity-width will be narrower the more face-on the galaxy is. Hence, some galaxies with inclinations close to the line of sight could be missed.

In this section, we use the sample of confirmed HIJASS sources to study the relative seriousness of these two selec-

tion effects on the composition of an HI-selected sample of galaxies and the implications this has for derivations of the HIMF and Ω_{HI} .

5.1 The expected distribution of galaxies in an HI-selected sample as a function of inclination angle

If the assumption that the 21-cm line of HI is always optically thin is correct, then the relationship between integrated HI flux from a galaxy, S_{Int} (in Jy km s^{-1}), and total HI mass, M_{HI} (in M_{\odot}), is given by

$$M_{\text{HI}} = 2.356 \times 10^5 S_{\text{Int}} D^2 \quad (4)$$

where D is the distance in Mpc (see e.g. Rohlfs 1986).

Now, if we assume that HI emission from any given type of galaxy is not necessarily optically thin, i.e. that there is an inclination-dependent opacity effect, then we can re-write equation (4) as

$$M_{\text{HI}} = 2.356 \times 10^5 S_{\text{Int}} D^2 f(i) \quad (5)$$

where $f(i)$ is the correction factor needed to correct the HI mass derived from the optically thin assumption to the actual HI mass. Assuming this function is significant at all, then $f(i)$ may vary for different morphological types and will increase as inclination angle increases.

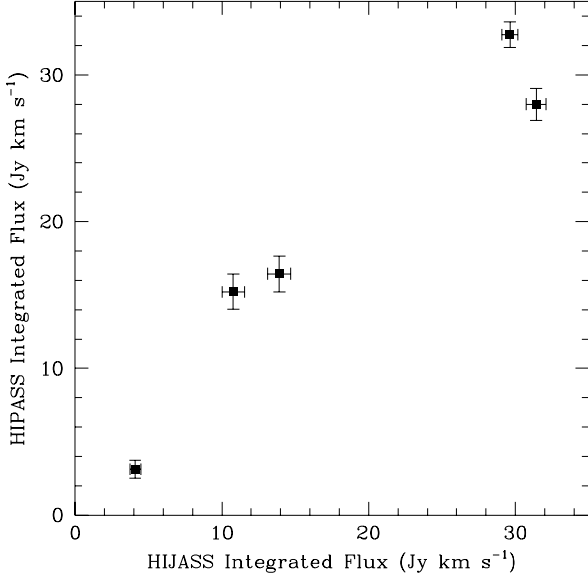


Figure 11. Comparison of integrated fluxes from HIJASS and HIPASS for galaxies in the region $12^h08^m \rightarrow 12^h34^m$, Decl.= $22^\circ \rightarrow 25^\circ$.

From eqn (5), it follows that the integrated flux, S_{Int} , which a galaxy of HI mass, M_{HI} , and inclination angle, i , will have at a distance of D can be written as:

$$S_{\text{Int}} = \frac{1}{2.356 \times 10^5} \cdot \frac{M_{\text{HI}}}{D^2} \cdot \frac{1}{f(i)} \quad (6)$$

Hence, if a survey has an integrated flux limit, $S_{\text{Int}}^{\text{lim}}$, then the maximum distance, D_{max} in Mpc, at which one could detect a galaxy of HI mass, M_{HI} , and inclination angle, i , would be given by

$$D_{\text{max}} = \left[\frac{1}{2.356 \times 10^5} \cdot \frac{M_{\text{HI}}}{f(i)} \cdot \frac{1}{S_{\text{Int}}^{\text{lim}}} \right]^{\frac{1}{2}} \quad (7)$$

However, as discussed in Section 4.2, the HIJASS sample does not have a single $S_{\text{Int}}^{\text{lim}}$ value. The sample is approximately peak flux limited and the integrated flux limit varies with velocity-width such that:

$$S_{\text{Int}}^{\text{lim}} \simeq 0.6 \Delta V_{20} S_{\text{pk}}^{\text{lim}} \quad (8)$$

So, for a given peak flux limit, the maximum distance at which a galaxy could lie and still be included in the HIJASS sample is related to its M_{HI} , ΔV_{20} and i , by:

$$D_{\text{max}} \propto \left[\frac{M_{\text{HI}}}{f(i)} \cdot \frac{1}{\Delta V_{20}} \right]^{\frac{1}{2}} \quad (9)$$

and the volume, $V(i)$ (in Mpc^3), within which such a galaxy could lie and still be included within HIJASS is related to M_{HI} , ΔV_{20} and i by:

$$V(i) \propto \left[\frac{M_{\text{HI}}}{f(i)} \cdot \frac{1}{\Delta V_{20}} \right]^{\frac{3}{2}} \quad (10)$$

Now, we expect galaxies to be randomly oriented in space. If so then the intrinsic distribution of galaxies as a function of inclination angle, $N(i)$, is described by

$$N(i) \propto \sin i \quad (11)$$

To find the expected observed distribution of galaxies as a function of inclination angle, $\phi(i)$, we have to multiply the intrinsic distribution of galaxies as a function of i , $N(i)$, by the volume within which a galaxy at a given i can be observed, $V(i)$, i.e.

$$\phi(i) \propto \left[\frac{M_{\text{HI}}}{f(i)} \cdot \frac{1}{\Delta V_{20}} \right]^{\frac{3}{2}} \cdot \sin i \quad (12)$$

The expected observed distribution of the HIJASS sample as a function of inclination angle therefore depends on several other relationships: the distribution of galaxies as a function of M_{HI} ; the relationship (if any) between M_{HI} and ΔV_o ; the relationship between ΔV_o and ΔV_{20} and inclination angle, i . In Section 5.3 we show that at large i (i.e. $>50^\circ$) this relationship can be simplified and used to study the effect of HI self-absorption within the HIJASS sample. Firstly, in Section 5.2, we consider the effect of the velocity-width limit on the HIJASS sample at small inclination angles.

5.2 Effect of the velocity-width limit on the HIJASS sample

For a given galaxy, ΔV_{20} is an observed property which depends on a combination of its rotational velocity, V_{rot} , its inclination to the line of sight, i , its internal velocity dispersion, ΔV_t (i.e. that due to turbulence and non-planar motions within the galaxy) and the contribution of instrumental broadening to the velocity width, ΔV_{inst} . For low M_{HI} galaxies, Tully & Fouque (1985) showed that these properties can be related via the equation:

$$\Delta V_{20} = [\Delta V_o^2 (\sin i)^2 + \Delta V_t^2]^{1/2} + \Delta V_{\text{inst}} \quad (13)$$

where $\Delta V_o = 2V_{\text{rot}}$ is the linewidth the galaxy would have if edge-on (i.e. ignoring the internal velocity-dispersion). For higher M_{HI} galaxies, the ΔV_t term adds linearly to the measured velocity-width (see also Verheijen & Sancisi 2001) since these galaxies generally show ‘boxy’ HI profiles rather than the typical Gaussian profiles of dwarf galaxies. However, since the velocity-width limit is more important for dwarf than giant galaxies, we conservatively adopt the quadratic summation of eqn(13).

If we assume that a galaxy cannot be seen by the survey if $\Delta V_{20} < \Delta V_{20}^{\text{lim}}$ then we can express the minimum inclination angle that a galaxy must have in order to be included in the sample as

$$i_{\text{min}} = \arcsin \left[\frac{(\Delta V_{20}^{\text{lim}} - \Delta V_{\text{inst}})^2 - \Delta V_t^2}{\Delta V_o^2} \right]^{1/2} \quad (14)$$

To illustrate the effect of the velocity-width limit, we adopt the value $\Delta V_t = 20 \pm 2 \text{ km s}^{-1}$ found by Rhee (1996) from a study of 28 galaxies with well defined HI velocity fields. This value is in close agreement with those found by similar studies by Broeils (1992) and Verheijen & Sancisi (2001). We use the Bottinelli et al. (1990) estimate of $\Delta V_{\text{inst}} = 0.55 \times R$, where R is the velocity resolution of the survey. This gives $\Delta V_{\text{inst}} = 10 \text{ km s}^{-1}$ for HIJASS. We assume $\Delta V_{20}^{\text{lim}} = 52.8 \text{ km s}^{-1}$ (see Section 4.2).

Table 4 illustrates the effect of the velocity-width cutoff on the number of galaxies included in the HIJASS sample for a range of ΔV_o values (Column 1). Column 2 lists the i_{min} for each ΔV_o , found using eqn(14) and our assumed

Table 4. Illustration of the effect of the velocity-limit selection effect on the inclusion of galaxies within the HIJASS sample. Column 1 is a set of ΔV_o values. Column 2 lists the minimum inclination angle, i_{min} , which a galaxy of each ΔV_o must have in order to be included in the sample (using eqn 14). Column 3 lists ζ , the fraction of galaxies which will be missed from the sample at each ΔV_o .

ΔV_o km s ⁻¹	i_{min} deg	ζ per cent
40	63.5°	55.4
50	49.2°	34.6
75	30.3°	13.7
100	22.2°	7.4
150	14.6°	3.2
200	10.9°	1.8
250	8.7°	1.2
300	7.3°	0.8
350	6.2°	0.6
400	5.4°	0.5

values above. As expected this effect gets progressively more serious for inherent narrow velocity-width objects: galaxies with $\Delta V_o < 100$ km s⁻¹ cannot be seen with $i < 22^\circ$; galaxies with $\Delta V_o < 50$ km s⁻¹ are missed if $i < 49^\circ$.

The actual fraction of galaxies missed at each ΔV_o can be found by integrating from $i=0$ to $i=i_{min}$ over a randomly oriented sample (see Zwaan et al., in preparation):

$$\zeta = \int_0^{i_{min}} \sin i \, di = 1 - \cos i_{min} \quad (15)$$

The derived values of ζ are listed in Column 3 of Table 4. Clearly, within HIJASS data, this selection effect becomes progressively more important at smaller ΔV_o . Whilst only 7% of galaxies have been missed at $\Delta V_o = 100$ km s⁻¹, this number has risen to 35% at $\Delta V_o = 50$ km s⁻¹.

As noted above, we cannot properly consider the effect that the velocity-width cut-off may have on a derived HIMF without knowing whether there is a relationship between ΔV_o and M_{HI} and, if so, what form that relationship takes. Whilst one could argue about the precise relationship between M_{HI} and ΔV_o , previous studies suggest that the two are related such that more massive galaxies appear to have broader velocity-widths. For example, from HI measurements of an optically-selected sample of galaxies, Rao & Briggs (1993) derived $\Delta V_{20} = 0.15 M_{HI}^{1/3}$. From their HIDEEP sample, Minchin et al. (in preparation) have found that $\Delta V_{20} = 0.42 M_{HI}^{0.28}$. However, such relations may be partly due to selection effects (see e.g. Minchin 2001).

Fig. 12 is a plot of ΔV_o against M_{HI} for 186 HIJASS galaxies for which we have derived inclination angles. This sample includes all of the previously catalogued galaxies (except those listed as ‘pair’ or ‘group’), the 15 ASSs for which the optical identification was relatively unambiguous (i.e. not the ASS*s) and the 5 PUGs for which an obvious optical counterpart could be seen on the DSS. The inclination for each galaxy was determined from the ratio of the semi-major to the semi-minor axis using the equation:

$$\cos^2 i = \frac{(b/a)^2 - r_o^2}{1 - r_o^2} \quad (16)$$

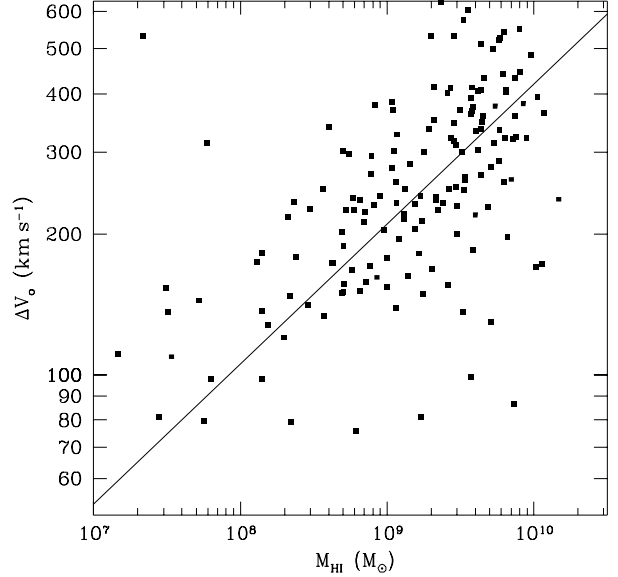


Figure 12. Plot of $\log(\Delta V_o)$ against $\log(M_{HI})$ for those 186 HIJASS galaxies for which we have inclination angles. The solid line is the locus of the relationship $\Delta V_o = 0.42 M_{HI}^{0.3}$ (equation 20).

(Holmberg 1958), where r_o is the intrinsic axis ratio of an edge-on disk. Estimates for r_o vary between 0.11 and 0.2 for this property. We have assumed a value of 0.16 for every galaxy. Note that this may be significantly inaccurate for low-mass dwarf galaxies, for which Staveley-Smith, Davies & Kinmann (1992) found that values up to about 0.5 may be appropriate. However, relatively few of the galaxies in the HIJASS sample are dwarfs (see Fig. 8a). The values of b/a were taken from the Third Reference Catalogue of Bright Galaxies (de Vaucouleurs et al. 1991) where available. Otherwise they were determined from DSS images of each galaxy using the SExtractor package (Bertin & Arnouts 1996).

Included on Fig. 12 is the locus of a line showing the relationship

$$\Delta V_o = 0.42 M_{HI}^{0.3} \quad (17)$$

which gives the best fit to our data. Note, however, that there is a wide scatter about this locus. There are very few data points at $M_{HI} < 10^8 M_\odot$ and many of these lie a long way from the locus of eqn 17. Hence, the conclusions we draw using this relationship, especially at low M_{HI} , should be treated as only illustrative of the possible effect of ignoring the velocity-width limit selection effect.

Table 5 lists the ΔV_o (Column 2) equivalent to a range of M_{HI} values (Column 1), assuming the ΔV_o - M_{HI} relationship of eqn(17). Also listed (Column 3) is the minimum inclination angle i_{min} which a galaxy of each ΔV_o could have and still be included in the HIJASS sample (assuming $\Delta V_{20}^{lim} = 52.8$ km s⁻¹) (from eqn.14). Column 4 lists the fractional error, ζ , which would be introduced into the HIMF at each mass as a result of the exclusion from the HI-selected sample of galaxies at $i < i_{min}$ (from eqn.15).

As is clear from Column 4 of Table 5, under these assumptions, for the HIJASS sample, we would be significantly underestimating the HIMF at $M_{HI} < 10^8 M_\odot$ if we did not compensate for the velocity-width limit selection

Table 5. Illustration of the effect of the velocity-limit selection effect on the HIMF derived from HIJASS data ($\Delta V_{20}^{\text{lim}}=52.8 \text{ km s}^{-1}$). Column 2 shows the ΔV_o value for a range of M_{HI} values (Column 1), derived assuming eqn (17) (note the caveats about this in the main body of the text). Column 3 shows the minimum inclination angle, i_{min} , at which a galaxy of this ΔV_o would be included in the sample (from eqn 14). Column 4 shows the percentage error in the HIMF at each mass resulting from excluding galaxies with $i < i_{\text{min}}$ (from eqn 15) from the sample.

M_{HI} M_{\odot}	ΔV_o km s^{-1}	i_{min} deg	ζ per cent
2×10^7	65	35.6	18.7
5×10^7	86	26.1	10.2
1×10^8	105	21.1	6.7
5×10^8	171	12.8	2.5
1×10^9	210	10.4	1.6
5×10^9	341	6.4	0.6
1×10^{10}	420	5.2	0.4

effect. What is most striking is that the extent of our underestimate of the HIMF would increase at the low M_{HI} /small ΔV_o end. This implies that HIMFs derived from HI-selected samples without correcting for this effect may have significantly underestimated the steepness of the faint-end slope. There are, however, other complicating factors which may affect the low mass end, e.g. the relationship of V_{rot} to velocity dispersion in dwarfs (e.g. Lo, Sargent & Young 1993, Staveley-Smith et al. 1992). At best, Table 5 is a warning that a consideration of the effect of the velocity-width cut-off on sample completeness should be an essential part of any derivation of the HIMF.

5.3 Effect of HI self-absorption

To study the possible impact of HI self-absorption on the HIJASS sample, we ideally wish to study the actual observed distribution of inclination angles of the sample against that predicted for a sample with no HI self-absorption. Eqn (12) describes the expected observed distribution of galaxies as a function of inclination angle, $\phi(i)$. As noted above, this is a complex function which depends on the relationship between ΔV_o and M_{HI} and that between ΔV_o and ΔV_{20} . However, if we restrict our analysis to large inclination angles then we can reasonably make two simplifying assumptions. The first is that we are not missing a significant number of galaxies due to the velocity-width limit selection effect. As noted in Table 4, only a galaxy with $\Delta V_o < 50 \text{ km s}^{-1}$ will be missed due to this effect at $i < 50^\circ$. The second is that at $i > 50^\circ$ the thermal velocity dispersion, V_t , no longer makes a significant contribution to V_{20} and, hence, we can assume that

$$\Delta V_{20} \simeq \Delta V_o \sin i \quad (18)$$

In this case, the expected observed distribution of galaxies as a function of i can be written as

$$\phi(i) \propto \left[\frac{M_{\text{HI}}}{\Delta V_o} \right]^{\frac{3}{2}} \cdot \left[\frac{1}{f(i)} \right]^{\frac{3}{2}} \cdot \left[\frac{1}{\sin i} \right]^{\frac{1}{2}} \quad (19)$$

Since M_{HI} and ΔV_o are constant for a given galaxy, the expected observed distribution of all galaxies in the HIJASS

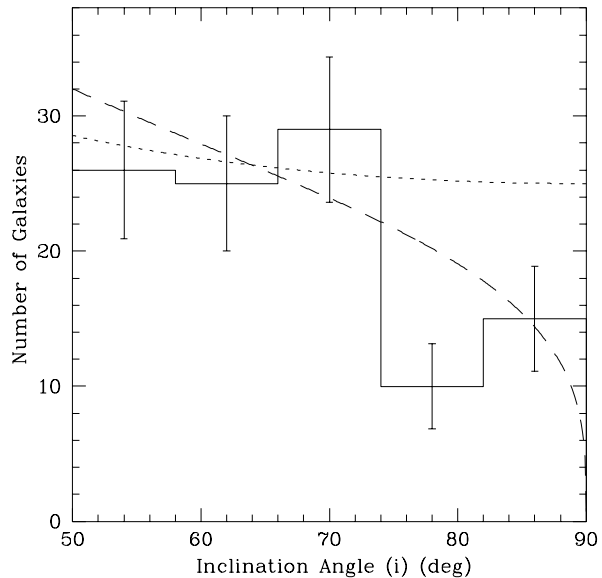


Figure 13. Histogram showing observed distribution of HIJASS galaxies as a function of inclination angle, i , for galaxies with $i > 50^\circ$. Each bin has width 8° . The short-dashed line shows a $\phi(i)$ function, fitted to the observed distribution in the range $i=50^\circ \rightarrow 74^\circ$ (assumes no self-absorption). The long-dashed line shows the best fitting $\phi(i)$ function to galaxies in the range $i > 50^\circ$ (assumes self-absorption with a best fit value of $\beta=0.2$).

sample as a function of inclination angle can then be described by

$$\phi(i) \propto f(i)^{-1.5} (\sin i)^{-0.5} \quad (20)$$

The implication of this equation is that, in the absence of significant self-absorption, we expect to see a relatively flat distribution at $i > 50^\circ$.

Fig. 13 presents a histogram of the derived inclination angles for those of the 186 HIJASS galaxies for which we have derived inclination angles where $i > 50^\circ$ (105 galaxies). In the optically thin scenario, we expect a very shallow fall-off in the observed distribution at high inclination angles. We actually observe a sharp fall in the observed number of galaxies at $i > 74^\circ$. This could be because self-absorption becomes significant in at least some galaxies at these high inclinations.

We can quantify the effect of self-absorption if we assume that the sample of galaxies in the range $i=50^\circ \rightarrow 74^\circ$ is free from the effects of both the velocity-width cut-off and HI self-absorption. Note that the velocity-width limit will tend to flatten the observed distribution as a function of i , so this assumption may lead to us underestimating the effects of self-absorption rather than over-estimating it. We have fitted a $\phi(i)$ function to the observed distribution in the range $i=50^\circ \rightarrow 74^\circ$. The best fit was determined by normalising $\phi(i)$ such that the theoretical number of galaxies in the range $i=50^\circ \rightarrow 74^\circ$ is equal to the observed number of galaxies in this range. The best fitting $\phi(i)$ function is plotted on Fig. 13 (short-dashed line).

This best fitting $\phi(i)$ distribution predicts that there should be 51 ± 7 galaxies at $i > 74^\circ$. This compares to the observed number of 25 galaxies, i.e. a 3.5σ shortfall of galaxies. An alternative fit can be made by normalising the theoret-

ical $\phi(i)$ function in the range $i=50^\circ \rightarrow 74^\circ$ to 1σ below the total observed counts in this range. Such a best fit predicts that there should be a total of 44 ± 7 galaxies at $i > 74^\circ$, still 2.5σ above the number observed.

The largest previous study of this issue was that of Haynes & Giovanelli (1984) who obtained HI measurements of 288 isolated galaxies using the Arecibo 305-m telescope. They compared the HI surface density (defined as the ratio of integrated HI flux to optical surface area of the galaxy) with the axial ratio for the galaxies as a function of morphological type. They found that for Sa, Sab, Sb, Sbc and Sc galaxies there was a clear trend for the measured surface density to fall as inclination to the line of sight increases. The implication of this is that the measured column depth of a highly inclined galaxy is less than it would be for more face-on objects because a fraction of the HI is being self-absorbed. Haynes & Giovanelli found a general trend for $f(i)$ [the inclination-dependent HI mass correction factor - see eqn (5)] to vary as

$$f(i) = (\cos i)^{-\beta} \quad (21)$$

where β is a constant dependent on morphological type. They found values of β of 0.04 for Sa and Sab, 0.16 for Sb, and 0.14 for Sbc and Sc galaxies. They found no corrections to be necessary for galaxies earlier than Sa or later than Sc, indicating self-absorption to be negligible in these types.

We adopt a similar form for $f(i)$ and used a χ^2 minimisation technique to derive the value of β which gives a best fit to our observed distribution at $i > 50^\circ$. This best fitting value is $\beta=0.2$. This ignores the possible dependence of β on morphological type. The $\phi(i)$ function derived using $\beta=0.2$ is shown on Fig. 13 (long-dashed line). This value is significantly larger than the largest value derived by Haynes & Giovanelli (1984). Note, however, that our model does not provide a particularly good fit to the data above $i=74^\circ$, especially in the bin centered at $i=78^\circ$. This may be a consequence of the relatively small total number of galaxies in our sample or of the assumed functional form of $f(i)$ not being appropriate.

Using the argument of Zwaan et al. (1997), the average effect of self-absorption on measured M_{HI} can be obtained by averaging $f(i)$ over a random distribution of inclinations.

$$\langle f(i) \rangle = \frac{\int_0^{\pi/2} (\cos i)^{-\beta} \sin i \, di}{\int_0^{\pi/2} \sin i \, di} = \frac{1}{1 - \beta} \quad (22)$$

giving a mean correction over all inclinations of $\langle f(i) \rangle = 1.25$ for $\beta=0.2$. We have no knowledge of how $f(i)$ varies with M_{HI} or morphological type. If it is uncorrelated with M_{HI} then the effect of this on the HIMF would be to shift galaxies of each mass to higher masses by an average factor of 1.25. This would lead to a corresponding increase in M_{HI}^* . The shape of the HIMF would be unaltered.

This correction factor of 1.25 to M_{HI}^* is a lower limit for two reasons. Firstly, we found a best fitting β -corrected $\phi(i)$ function by assuming that the velocity-width limit effect was not significant at $i > 50^\circ$. As is clear from Table 4, some intrinsically narrow velocity-width galaxies will be lost even at $i > 50^\circ$. Hence, our value of β is a lower limit. Secondly, in deriving $\langle f(i) \rangle$ we have averaged over all i . We should actually integrate over $i=i_{\text{min}} \rightarrow 90^\circ$ for any given ΔV_o (since galaxies at $i < i_{\text{min}}$ will not have been included in

the sample). This would have the effect of increasing $\langle f(i) \rangle$ for those galaxies actually included in the sample.

We also have to account for the fact that self-absorption is not only causing us to underestimate the mass of some galaxies, but is also causing some galaxies to be excluded from the sample altogether. In a randomly oriented sample of galaxies, 28 per cent of the contribution to the HIMF should come from galaxies with $i > 74^\circ$. However, at $i > 74^\circ$ we are missing at least 40 per cent of those galaxies which we would expect to see in the absence of self-absorption. If we assume that self-absorption is not correlated with ΔV_o or M_{HI} then this effect will cause us to underestimate the HIMF by a factor of 1.14 at each M_{HI} , i.e. to derive the correct HIMF we would need to correct the normalisation θ^* by a factor of at least 1.14. The combined effect of the correction factors of 1.25 in M_{HI}^* and 1.14 in θ^* would be to increase the derived value of Ω_{HI} by at least 25 per cent.

Experience in the optical suggests that correcting for the number of self-absorbed discs in a survey, using only those you can see, is extremely model-dependent (Disney, Davies & Phillipps 1989; Witt, Thronson & Capuano 1992). For instance, in the present case the optical depth could vary by an order of magnitude as between flat and solid rotation curves. All we can truly say for now is that an HI-select survey like ours would, of all surveys, be most likely to run into HI self-absorption, and that the affect is plainly significant. How significant remains a question for the future.

6 CONCLUDING REMARKS

This paper has described the properties of the present sample of confirmed sources derived from the HIJASS data. This sample will be added to as further sources are confirmed. This will obviously follow further observing runs on the Lovell telescope. However, there is scope within existing HIJASS data for adding to the present sample. As noted in Section 3.1, the ‘possible’ detections from the 2002 run have not yet been followed up by single-beam narrow-band observations. Those confirmed in this way will then be added to the sample. We noted in Section 4.2 the important selection effect that, because our sample is effectively peak flux limited, the integrated flux limit is a function of ΔV_{20} . This leads to a major bias against galaxies with broad velocity-widths (and presumably higher HI masses). We are developing alternative detection techniques with the aim of detecting broader velocity-width sources to similar integrated flux levels as we can presently detect narrow-line sources. There is a further possibility that nearby spatially extended objects may be removed from the data by the conventional bandpass correction algorithm used by LIVEDATA. Alternative algorithms are being tested to determine if any sources have been lost in this way. We are also considering ways of detecting massive galaxies in the data between $cz=7500-9000 \text{ km s}^{-1}$. It is possible that any galaxies massive enough to be detectable at this distance will have very broad velocity-widths and hence, be hard to actually detect despite their mass.

We have embarked upon a detailed follow-up program in order to fully study the astrophysical nature of the objects within the HIJASS sample: in particular the previously uncatalogued objects. As discussed in Section 1, the addition of these previously uncatalogued objects to the extra-

galactic census of the local Universe could have a significant impact not only on determinations of the luminosity density and mass density of the local universe but also on our understanding of the processes of galaxy formation and evolution. They could be systems which have undergone a very different formation process and/or evolutionary path than optically selected galaxies. Are they old galaxies which have evolved slowly and have yet to transmute most of their gas into stars? Or are they young objects which are still at an early stage of their star formation histories? Are they objects which have recently accreted large amounts of HI? To determine this we require information on their morphological and structural properties; on their stellar populations; and on their star formation rates, star formation histories and metallicities. All of the potential new detections will be observed using the Westerbork Synthesis Radio Telescope (WSRT) in order to get accurate positions for these objects and to map the distribution of HI within them. This will also enable us to decide which of the 23 objects lying close to a catalogued galaxy with no measured redshift (ASSs) are actually associated with that previously catalogued galaxy and which are new objects. Broad band imaging is being undertaken with the Isaac Newton Telescope of the most interesting objects. We are attempting to detect H α emission from the nearer of the objects using the Jakobus Kapteyn Telescope. We have also been awarded time on the William Herschel Telescope to obtain IR imaging of several of the objects. Future publications will present the results of this follow-up program.

We have shown, using the HIJASS sample, that self-absorption is a significant, but often overlooked, effect in galaxies at high inclinations. Properly accounting for it could increase the derived HI mass density by at least 25 per cent and possibly a lot more. The effect this will have on the shape of the HIMF will depend on how self-absorption affects galaxies of different ΔV_o .

We have also shown that the velocity-width limit will always act so as to exclude low inclination angle galaxies from HI-selected samples. This effect will become progressively more serious at lower ΔV_o values. If, as we might expect, galaxies with smaller intrinsic velocity-widths have smaller HI masses, then compensating for this effect could significantly steepen the faint end of the HIMF.

ACKNOWLEDGMENTS

The construction of the multibeam receiving system at Jodrell Bank was made possible by the UK PPARC (Grant No. GR/K28237 to Jodrell Bank). The HI Jodrell All Sky Survey is funded by the UK PPARC (Grant No. PPA/G/S/1998/00620 to Cardiff). Both grants are gratefully acknowledged. PJB and RFM also acknowledge the financial support of the UK PPARC. We thank the Director of the Jodrell Bank Observatory, Prof. Andrew Lyne, for granting the observing time for HIJASS and for making available the facilities of the observatory. We thank CSIRO Radiophysics in Australia for producing much of the design and engineering of the system. We also thank the following for their help with HIJASS: Gareth Banks, Dave Brown, Mark Calabretta, Jim Cohen, Jon Davies, Rod Davies, Judy Haynes, Anthony Holloway, Ian Morison, Rhys Morris, Rod-

ney Smith, Lister Staveley-Smith, Daniel Zambonini and the staff and students of the Jodrell Bank Observatory. This research has made use of the NASA/IPAC Extragalactic Database (NED) which is operated by the Jet Propulsion Laboratory, Caltech, under agreement with the National Aeronautics and Space Administration. This research has also made use of the Digitised Sky Survey, produced at the Space Telescope Science Institute under US Government Grant NAG W-2166.

REFERENCES

- Banks G.D., et al., 1999, ApJ, 524, 612
 Barnes D.G. et al., 2001, MNRAS, 322, 486
 Baugh C., Cole S., Frenk C.S., 1996, MNRAS, 283, 1361
 Bertin E., Arnouts S., 1996, A&AS, 117, 393
 Bell E.F., Bower R.G., 2000, MNRAS, 319, 235
 Bell E.F., de Jong R.S., 2000, MNRAS, 312, 497
 Bird T.S., 1994, in IEEE Antennas & Propagation Symposium. Seattle, p.966
 Bird T.S., 1997, in IEEE Antenna & Propagation Society Symposium, Montreal, p. 1618
 Bottinelli L., Gouquenheim L., Fouque P., Paturel G., 1990, A&AS, 82, 391
 Boyce P.J. et al., 2001, ApJ, 560, L127
 Broeils, A.H., 1992, PhD Thesis, Univ Groningen
 Canaris J., 1993, in Workshop on New Generation Digital Correlators. Publisher, Tuscon, p.117
 Cross N.J.G., et al., 2001, MNRAS, 324, 825
 Disney M.J., 1976, Nature, 263, 573
 Disney M.J., 1999, in Davies J.I., Impey C., Phillipps S., eds, Low Surface Brightness Universe, ASP, San Francisco
 Disney M.J., Phillipps S., 1987, Nature, 329, 203
 Disney M.J., Davies J.I., Phillipps S., 1989, MNRAS, 239, 939
 Epstein E.E., 1964a, AJ, 69, 490
 Epstein E.E., 1964a, AJ, 69, 512
 Freedman W.L. et al., 1994, ApJ, 427, 628
 Gooch, R., 1995, in ASP Conf. Ser. 77: ADASS IV, Volume 4
 Haynes M.P., Giovanelli R., 1984, 89, 758
 Holmberg E., 1958, Medd.Lunds.Astr.Obs., Ser.II, No.136
 Impey C.D., Bothun G.D., 1997, ARA&A, 35, 267
 Impey C.D., Bothun G.D., Malin D.F., 1988, ApJ, 330, 634
 Kauffmann G., Nusser A., Steinmetz M., 1997, MNRAS, 286, 795
 Kilborn V.A., 2000, PhD thesis, Univ Melbourne
 Kilborn V.A. et al., 2000, AJ, 120, 1342
 Kilborn V.A. et al., 2002, AJ, 124, 690
 Lo K.Y., Sargent W.L.W., Young K., 1993, AJ, 106, 507
 McGaugh S.S., 1996, MNRAS, 280, 337
 Minchin R.F., 2001, PhD thesis, Univ. Wales, Cardiff
 Phillipps S., Disney M.J., Kibblewhite, E., Cawson M.G.M., 1987, MNRAS, 229, 505
 Rao S., Briggs F.H., 1993, ApJ, 36, 267
 Rhee, M.-H., 1996, A&AS, 115, 407
 Rohlfs K., 1996, Tools of Radio Astronomy, Springer-Verlag
 Rosenberg J.L., Schneider S.E., 2002, ApJ, 567, 247
 Rosenberg J.L., Schneider S.E., 2000, ApJS, 130, 177
 Ryan-Weber E. et al., 2002, AJ, 124, 1954
 Ryder S.D. et al., 2001, ApJ, 555, 232
 Sault R.J., Teuben P.J., Wright M.C.H., 1995, ADASS, p.433, ASP San Francisco
 Schneider S.E., Spitzak J.G., Rosenberg J.L., 1998, ApJ, 507, L9
 Solanes J.M., Giovanelli R., Haynes M.P., 1996, ApJ, 461, 609
 Sorar E., 1994, PhD Thesis, Univ Pittsburgh
 Spitzak J.G., Schneider S.E., 1998, ApJS, 119, 159
 Staveley-Smith L., Davies R.D., Kinmann T.D., 1992, 258, 334

- Staveley-Smith L. et al., 1996, Proc. Astron. Soc. Australia, 13, 243
- Tully R.B., Fouque., 1985, ApJS, 58, 67
- de Vaucouleurs G., de Vaucouleurs A., Corwin H.G., Buta R.J., Paturel G., Fouque P., 1991, Third Reference Catalogue of Bright Galaxies, Springer-Verlag, New York
- Verheijen M.A.W., Sancisi R., 2001, A&A, 370, 765
- Witt A., Thronson H.A., Capuano J.M., 1992, ApJ, 393, 611
- Zwaan M.A., Briggs F.H., Sprayberry D., Soror, E., 1997, ApJ, 490, 173